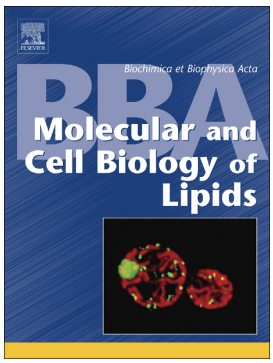
Journal Pre-proof



Lipolysis and lipophagy play individual and interactive roles in regulating triacylglycerol and cholesterol homeostasis and mitochondrial form in zebrafish

Si-Lan Han, Yu-Cheng Qian, Samwel Mchele Limbu, Jing Wang, Li-Qiao Chen, Mei-Ling Zhang, Zhen-Yu Du

PII: S1388-1981(21)00116-5

DOI: https://doi.org/10.1016/j.bbalip.2021.158988

Reference: BBAMCB 158988

To appear in: *BBA - Molecular and Cell Biology of Lipids*

Received date: 25 February 2021

Revised date: 29 May 2021

Accepted date: 3 June 2021

Please cite this article as: S.-L. Han, Y.-C. Qian, S.M. Limbu, et al., Lipolysis and lipophagy play individual and interactive roles in regulating triacylglycerol and cholesterol homeostasis and mitochondrial form in zebrafish, *BBA - Molecular and Cell Biology of Lipids* (2021), https://doi.org/10.1016/j.bbalip.2021.158988

This is a PDF file of an article that has undergone enhancements after acceptance, such as the addition of a cover page and metadata, and formatting for readability, but it is not yet the definitive version of record. This version will undergo additional copyediting, typesetting and review before it is published in its final form, but we are providing this version to give early visibility of the article. Please note that, during the production process, errors may be discovered which could affect the content, and all legal disclaimers that apply to the journal pertain.

© 2021 Elsevier B.V. All rights reserved.

Lipolysis and lipophagy play individual and interactive roles in regulating triacylglycerol and cholesterol homeostasis and mitochondrial form in zebrafish

Si-Lan Han,[1] Yu-Cheng Qian,[1] Samwel Mchele Limbu,[2] Jing Wang,[1] Li-Qiao Chen,[1] Mei-Ling Zhang,[1] Zhen-Yu Du[1,*]

[1]LANEH, School of Life Sciences, East China Normal University, Shanghai, China

[2]University of Dar es Salaam, P.O. Box 60091, Dar es Salaam, Tanzania

*Correspondence: zydu@bio.ecnu.edu.cn

Journal Pre-proof

Abstract

Neutral lipases-mediated lipolysis and acid lipases-moderated lipophagy are two main processes for degradation of lipid droplets (LDs). However, the individual and interactive roles of these metabolic pathways are not well known across vertebrates. This study explored the roles of lipolysis and lipophagy from the aspect of neutral and acid lipases in zebrafish. We established zebrafish strains deficient in either adipose triglyceride lipase (*atgl*$^{-/-}$; AKO fish) or lysosomal acid lipase (*lal*$^{-/-}$; LKO fish) respectively, and then inhibited lipolysis in the LKO fish and lipophagy in the AKO fish by feeding diets supplemented with the corresponding inhibitors Atglistatin and 3-Methyladenine, respectively. Both the AKO and LKO fish showed reduced growth, swimming activity, and oxygen consumption. The AKO fish did not show phenotypes in adipose tissue, but mainly accumulated triacylglycerol (TAG) in liver, also, they had large LDs in the hepatocytes, and did not stimulate lipophagy as a compensation response but maintained basal lipophagy. The LKO fish reduced total lipid accumulation in the body but had high cholesterol content in liver; also, they accumulated small LDs in the hepatocytes, and showed increased lipolysis, especially Atgl expression, as a compensatory mechanism. Simultaneous inhibition of lipolysis and lipophagy in zebrafish resulted in severe liver damage, with the potential to trigger mitophagy. Overall, our study illustrates that lipolysis and lipophagy perform individual and interactive roles in maintaining homeostasis of TAG and cholesterol metabolism. Furthermore, the interactive roles of lipolysis and lipophagy may be essential in regulating the functions and form of mitochondria.

Keywords:

Lipolysis; Lipophagy; Interaction; Lipid catabolism; Mitochondria; Zebrafish

Journal Pre-proof

1. Introduction

Intracellular lipid droplets (LDs) are dynamic and complex organelles consisting of core neutral lipids, including triacylglycerol (TAG) and cholesterol esters (CE), encircled by a phospholipid monolayer [1,2]. LDs perform essential functions in energy metabolism by regulating lipid storage and release [3]. Lipolysis and lipophagy are currently recognized as the two main processes for LDs degradation in mammals [4]. The former works through an adipose triglyceride lipase (ATGL)–hormone sensitive lipase (HSL)–monoacylglycerol lipase (MGL) cascade pathway to break down TAGs [5]. In this pathway, ATGL (also known as PNPLA2) is regarded as a key hydrolase, expressed in virtually all tissues [6] but particularly in adipose tissue [7]. Although adipose tissue is usually regarded as the main site of ATGL functions, specific knockout of ATGL caused hepatic steatosis, suggesting that ATGL might also play important roles in the liver [8]. Owing to its vital roles, individuals without functional ATGL developed neutral lipid storage disease with myopathy (NLSDM) [9-11], whereas ATGL-null mice had impaired release of fatty acids (FAs) and ectopic lipid accumulation [12]. Besides lipolysis, LDs can also become trapped in double-membrane vesicles and subsequently fuse with lysosomes for degradation during a process called lipophagy [13]. Lysosomal acid lipase (LAL) is the most important lipase in lysosomes and participates in lipophagy at a pH of 4 to 5 [14]. Some researchers regard lipophagy as an "acid lipolysis" owing to the suitable pH level, as opposed to neutral lipolysis achieved by using other lipases [15,16]. The loss of lipophagy or autophagy-related genes in mammals can result in severe health consequences. For instance, LAL deficiency in humans caused Wolman disease or cholesteryl ester storage disease [17,18]. In mice, knockdown of ATG5 (an autophagy-related gene) in liver cells, and liver-specific ATG7 deletion, both induced accumulation of hepatic TAGs [13]. Moreover, *Lal*$^{-/-}$ mice developed severe hepatosplenomegaly and steatohepatitis [19,20]. Despite their important roles in degrading LDs, the individual contributions of lipolysis and lipophagy in total lipid metabolism, especially *in vivo*, have not yet been investigated.

Recent studies indicate that lipolysis and lipophagy may interact in terms of certain functions [21,22], depending on the tissues, cell types or physiological conditions [23]. For example, cold-induced autophagy facilitated lipolysis via microtubule associated light chain 3 (LC3) coupled with ATGL in brown adipocytes

[21]. The PNPLA5, a member of the family of patatin-like phospholipase domain-containing proteins that mobilize neutral lipids, was required for optimal autophagy initiation in HeLa cells [24]. Furthermore, ATGL regulated autophagic flux in hepatocytes [22] and promoted SIRT1, which is a major driver of autophagy [25]. Some researchers have suggested that lipophagy, as a downstream factor, is responsible for a large portion of LDs breakdown rather than ATGL or related lipases [26]. Although interactions between the processed of lipolysis and lipophagy are still unclear, the release of fatty acids in starved mammalian hepatocytes with low neutral lipase activities through lipophagy may be notable [13]. Nevertheless, there remains inadequate scientific evidence of how lipolysis and lipophagy interact or work in tandem in systemic lipid metabolism, partly because the compensatory effects of lipolysis or lipophagy have not be thoroughly studied when either one of the processes is blocked.

Zebrafish have become an important animal model for studies of metabolism. Fatty liver disease caused by a high-energy diet often occurs in fish, similarly as in mammals [27-29]. It has been confirmed that fish also possess the Atgl-Hsl-Mgl lipolytic cascade, and the genes encoding for Atgl are highly conserved between teleost and mammals [30-32]. Biochemical inhibition of Atgl by Atglistatin resulted in TAG accumulation and reduced fatty acid β-oxidation in zebrafish [33]. In addition, our earlier studies verified the existence of lipophagy in fish liver [34,35], while the inhibition of lipophagy retarded growth and caused inflammation [36,37]. Interestingly, some authors demonstrated that lipolysis-related genes, including *atgl*, are more highly expressed in fish liver than in adipose tissue [31,38], indicating that neutral lipases might be more active in fish liver. Therefore, fish is a good model to investigate the separate and interactive roles of lipolysis and lipophagy, especially in the liver where both processes exist.

In the present work, we established *atgl*$^{-/-}$ (AKO fish) and *lal*$^{-/-}$ (LKO fish) mutant zebrafish using the CRISPR/Cas9 gene-editing tool, to compare the separate roles of lipolysis and lipophagy based on neutral and acid lipases perspectives. Furthermore, we inhibited autophagy and lipolysis by administering 3-Methyladenine (3MA) and Atglistatin (AI) to the AKO and LKO zebrafish, respectively, to further explore the metabolic responses in fish when the two processes are simultaneously inhibited. During the study, we measured the oxygen consumption, fish body

composition, lipid classes, tissue damage and mitochondrial indexes, as well as several genes and proteins related to lipolysis and lipophagy. The present study advances our understanding of the roles of lipolysis and lipophagy in systemic lipid metabolism across species.

2. Materials and methods

2.1 Animal ethics

All animal experiments were conducted according to the Guide for the Care and Use of Laboratory Animals formulated by the Ministry of Science and Technology of China. This study was approved by the Committee on the Ethics of Animal Experiments of East China Normal University (Approval ID: F20190101).

2.2 Animal source and maintenance

All zebrafish (wild-type line: AB; CZRC Catalog ID: CZ1) were obtained from China Zebrafish Resource Center in Wuhan, China. Fish were maintained in a recirculating system, at 28 °C, with a light: dark cycle of 14 h: 10 h. Embryos were obtained through natural spawning and then kept in Petri dishes with static water at 28 °C. After 15 days post-fertilization, the fish larvae were transferred to a recirculating system and fed twice a day with freshly hatched *Artemia salina*.

2.3 Establishment of *atgl* and *lal* mutant zebrafish lines

The *pnpla2* mutant ($atgl^{-/-}$, AKO) and *lipf* mutant ($lal^{-/-}$, LKO) zebrafish were generated using the CRISPR/Cas9 tool, as described in our previous study [39]. Because the important functional domains of these two genes are located in the first few exons, the first exon was selected, and the target sites were designed using the ZiFiT Targeter software package (http://zifit.partners.org/ZiFiT). The mutation locus was then confirmed by genomic DNA sequencing. The resultant F3 AKO, LKO, and wild-type (WT) zebrafish were used for the experiment. However, we could not obtain the AKO-LKO double-mutant zebrafish yet, because they all died during the larval stage in our preliminary studies.

2.4 Experimental design

The experiment was done in two stages. First, to determine the general phenotype of

the AKO and LKO zebrafish, regardless of sex, 2-month-old juveniles of AKO, LKO, and their corresponding WT zebrafish (i.e. 4 groups), each with three replicates (i.e. 3 tanks per group, 12 total tanks, and 20 fish of the same genotypes per tank), were first fed a formulated basal diet (see Supplementary Table 1) at 4% body weight per day for 7 weeks. Next, because the first stage clearly indicated significant TAG in the liver of AKO fish and cholesterol deposition in LKO fish, we devised a second-stage which focused on liver metabolism, using only male fish of a larger size (3-months-old) so as to collect sufficient samples of liver and to avoid the effect of sex. In this 4-week feeding trial, the AKO and LKO fish were fed the basal diet supplemented with or without the autophagy inhibitor (3-Methyladenine [3MA], HY-19312) or Atgl inhibitor (Atglistatin [AI], HY-15859), respectively, both of which were purchased from MedChemExpress. Thus, there were six groups (18 tanks in total: AKO, AKO+3MA, LKO, LKO+AI, and the corresponding WT of AKO and LKO fish; with 3 tanks per group, and 30 fish of the same treatment in each tank) to investigate the outcome of simultaneous inhibition of lipolysis and lipophagy. The dose of AI (80 mg/kg diet) was set according to our previous study [33], and that of 3MA (7.5 g/kg diet) was determined based on the preliminary study (see Supplementary Figure 1A).

The AI or 3MA was added to small wheat-dough particles. To prepare these inhibitor-containing particles, AI or 3MA was first dissolved in dimethyl sulfoxide (DMSO) and the solution was mixed with an appropriate amount of wheat flour and water to make a wet dough. The wet dough was shaped into small pieces of a suitable size for feeding to zebrafish, and then dried in an oven at 60 ℃. During the 4-week experiment, fish were fed three times per day (9:00, 14:30 and 18:30), with the daily rate of feed for all fish set at 4% body weight (1% wheat-dough particles + 3% basal diet) to achieve the same dose intake of inhibitors. The inhibitor-containing particles was given to fish fasted overnight before feeding with the basal diet each morning; typically, the zebrafish quickly ate the wheat-dough particles (within seconds) and consumed the basal diet entirely within ~20 minutes. During both stages of the experiment, the water temperature was 28 ± 1 ℃, dissolved oxygen in the range 6.5–7.5 mg/L, pH 7.5 ± 0.5, and total ammonia nitrogen <0.02 mg/L. The weight of all fish in each tank was recorded every week, and the amount of feed was adjusted accordingly.

177 **2.5 Swimming activity and oxygen consumption rate (OCR)**

178 Movement behavior was measured using automated live video tracking (ZebraLab
179 software; ViewPoint Life Sciences, Lyon, France) of six randomly selected fish in
180 each replicate tank, according to the method in our previous study [40]; swimming
181 activity was calculated as the total distance traveled during the video recording period.
182 The oxygen consumption rate (OCR) was determined with a dissolved oxygen
183 respirometer (Strathkelvin 782 Oxygen System; North Lanarkshire, Scotland, UK): 30
184 zebrafish of each genotype (AKO, LKO, and their WT siblings) were fasted overnight
185 and then transferred to an oxygen-saturated water chamber; OCR was expressed as
186 milligrams of O_2 consumed per hour per body weight.
187

188 **2.6 Biochemical analyses**

189 The concentrations of triglyceride (TAG), total cholesterol (TC), low density
190 lipoprotein cholesterol (LDL-C), and free fatty acid (FFA) in the liver of six fish from
191 each treatment were assessed using commercial kits (Jiancheng Biotechnology Co.,
192 China). Phospholipid (PL) was measured from six fish in each treatment using an
193 ELISA kit (Shanghai Jining Shiye Co., China). The Atgl, Hsl and Lal enzyme
194 contents were likewise detected using ELISA kits (Shanghai Yifei Biotech Co., China).
195 Whole fish protein from six fish in each treatment was determined with a Kjeltec
196 2300 Analyzer Unit (FOSS Tecator, Hoganas, Sweden) after acid digestion. The total
197 lipid of six whole fish in each treatment was extracted using chloroform/methanol
198 (2:1, v/v) and the lipid classes were separated from total lipids by thin-layer
199 chromatography. Six samples in each group for fatty acid (FA) assay were prepared
200 using boron trifluoride in methanol (14%) solution for the fatty acid methyl esters
201 (FAMEs) derivatization, as described previously [41]. The FAMEs samples were
202 analyzed with a gas chromatograph (GC-2010, Shimadzu Corp., Japan) connected to a
203 chromatography column (Restek column: 100-m length, 0.25-mm internal diameter,
204 0.2-μm film thickness). The carrier gas was high-purity nitrogen at a flow rate of 7.8
205 ml/min. The injector and detector temperatures were set at 250 °C and 260 °C,
206 respectively. Fatty acids were identified by retention times from standard mixtures
207 (Supelco CRM47885). The FA data were expressed as the area percentage of FAMEs.
208

209 **2.7 Histological, tissue immunofluorescence assays and transmission electron**

microscopy (TEM) analyses

Six pieces of fish livers from each treatment were fixed in 4% paraformaldehyde solution and then embedded in paraffin. Sections of 5-μm thickness were stained with Harris's hematoxylin–eosin mixture, as done in our previous study [42]. Another unstained six liver sections were used for immunofluorescence, as described in our earlier study [33]; the antibodies used in this experiment were anti-LAMP1 (Abcam catalog #ab24170), anti-LC3A/B (CST #4108) and anti-HSP60 (Affinity catalog #AF5374). Six liver samples from zebrafish were collected and immediately fixed with TEM fixative (G1102, Servicebio) for 2 to 4 h. The samples were then processed as described previously [39]. Images were obtained using a Hitachi HT7700 Transmission Electron Microscope (Hitachi High-Tech Corp., Tokyo, Japan).

2.8 Quantitative real-time PCR and mtDNA measurements

The extraction of total RNA from liver samples of six fish, cDNA synthesis and quantitative real-time PCR were performed as described previously [33]. The house-keeping genes elongation factor 1 alpha (*ef1α*) and *β-actin* were used as the reference genes, which were expressed stably among treatments. The primers of genes for qPCR were designed to overlap introns (Supplementary Table 2). The method of $2^{-\Delta\Delta Ct}$ was used for estimating the relative cDNA abundance. Total mitochondrial DNA (mtDNA) of liver was extracted using a TIANamp Marine Animals DNA Kit (Tiangen Biotech Co., China) following the manufacturer's instructions. The relative copy number of mtDNA was measured by qRT-PCR. Details of the primers used for the mtDNA are provided in Supplementary Table 3.

2.9 Western blotting

Western blotting was performed using liver homogenates, following the method we previously reported [33]. The antibodies used in the present study were anti-Lc3A/B (1:800, #4108, CST), anti-Beclin1(1:800, 11306-1-AP, Proteintech), anti-P62 (1:800, #5114, CST), anti-Lal (1:500, Custom Antibody Services from HuaAn Biotech, China), anti-Atgl (1:500, Custom Antibody Services from HuaAn Biotech, China), anti-Hsl (1:800, #4107, CST), anti-p-Hsl (Ser552) (1:800, D151508, BBI), and anti-Gapdh (1:3000, AB0036, Abways). The Western blot images were obtained with an Odyssey CLx Imaging System (LI-COR, USA).

2.10 Transcriptomic analysis

The RNA for sequencing was collected from six whole fish per treatment (WT/AKO and WT/LKO) in the first stage of the experiment, using TRIzol Reagent according to the manufacturer's recommendations (Invitrogen, Carlsbad, CA, USA). After RNA extraction, purification and construction of the transcriptome library, paired-end (PE) reads were obtained by next-generation sequencing (NGS) using an Illumina HiSeq platform. After filtering out low quality reads, the remaining clean reads were aligned to the zebrafish reference genome (Database version: 96.11) using TopHat2. Differentially expressed genes (DEGs) were calculated according to the fragments per kilobase of exon per million mapped reads (FRKM) method. Using Blast2GO and KAAS software, functional-enrichment analysis, including Gene Ontology (GO) and Kyoto Encyclopedia of Genes and Genomes (KEGG), was performed to identify the DEGs that were significantly enriched in GO terms and in metabolic pathways, at Bonferroni-corrected *p*-value of ≤0.05, compared with the whole-transcriptome background.

2.11 Statistical analyses

All data are presented as mean ± standard error of the mean (SEM) and assessed by one-way ANOVA or using a Student's t-test. When ANOVA showed significant differences, comparisons between means were determined by Tukey's multiple range test ($p < 0.05$). All analyses were conducted by using IBM SPSS Statistics 19 software (SPSS, Michigan Avenue, Chicago, IL, USA).

3. Results

3.1 AKO zebrafish showed retarded growth, protein loss, and severe lipid deposition

The *pnpla2* encodes a protein comprising 486 amino acids, and the knockout line (*atgl*$^{-/-}$/AKO) was generated by deleting 5 base pairs (bp) in its first exon. As expected, the putative translation product had a premature stop codon and it consisted of only 71 amino acids (Figure 1A). In the 7-week feeding trial, the AKO zebrafish showed retarded growth (Figure 1B), weakened swimming activity (Figure 1C), and lower

respiration rate (Figure 1D) when compared with the WT fish. Furthermore, the AKO fish had significantly lower whole body protein content than the WT fish (Fig. 1E) but exhibited significant increases in total lipid content (Figure 1F) and viscera somatic index (VSI) (Figure 1G). Moreover, TAG content, but not phospholipid (PL) content, was markedly increased in the AKO fish (Figure 1H, I). Accordingly, the AKO fish contained higher percentages of TAG but less PE and PC in the total lipids than in the WT fish (Figure 1J). Additionally, the AKO zebrafish had higher percentages of C16:1, C18:1n-9, and C18:3n-6, but lower percentages of C24:1 and C22:6n-3 as compared with the WT fish (Figure 1K). The liver of AKO zebrafish was white, and its histological image showed many more vacuoles, indicating fat accumulation, than seen in the bright red liver of WT fish (Figure 1L). Together, these results reveal growth retardation, low metabolic rate and severe lipid (TAG) deposition in the AKO zebrafish.

3.2 LKO zebrafish differed in their lipid profile and fatty acid composition

The *lipf* at first encodes a protein comprised of 396 amino acids. The *lal*$^{-/-}$/LKO zebrafish generated by the CRISPR/Cas9 tool lost 5 bp in the first exon. As expected, the putative translation product had a premature stop codon and consisted of only 30 amino acids (Figure 2A). The LKO mutants likewise presented slower growth (Figure 2B), less swimming ability (Figure 2C), and a lower OCR (Figure 2D) than the WT fish, together with an increased VSI (Figure 2E) and decreased protein content (Figure 2F). However, both the total lipid (Figure 2G) and TAG (Figure 2H) decreased significantly in LKO fish when compared with WT fish, but without affecting whole fish PL content (Figure 2I). Accordingly, the percentage of TAG decreased while the percentages of CE, PE, and PC increased in the total lipids of LKO fish (Figure 2J). Moreover, LKO fish had higher percentages of very long-chain polyunsaturated fatty acid (VLCPUFA), such as C20:5n-3 and C22:6n-3, but lower percentages of C16:0, C18:1n-9 and C18:2, as compared with the WT fish (Figure 2K). Surprisingly, LKO zebrafish had yellow liver with small, dense vacuoles (Figure 2L). To summarize, the Lal mutation appeared to reduce metabolic rate and body lipid content but increase the percentages of CE, PL, and VLCPUFA.

3.3 The AKO and LKO zebrafish displayed different lipid metabolism patterns

To clearly understand the effects of Atgl and Lal deficiency on lipid metabolism, the AKO, LKO, and their corresponding WT fish were used to perform transcriptome analysis (Supplementary Figure 2A-B). The data showed that lipid metabolism was the most-influenced biological process (Supplementary Figure 2A-iv, 2B-iv), and thus we filtered the DEGs related to lipid metabolism (Supplementary Figure 2C-E), as summarized in Figure 3. The results indicated that the loss of Atgl hindered TAG metabolism, including the downregulation of TAG synthesis genes (*dgat2* and *mogat3a*) and lipid catabolism genes (*fads2*, *elovl2*, *acsbg1*, *ehhadh* and *acaa1/2*), including the significant reduction of hepatic lipase gene, *lipca*. These findings correspond to the severe TAG accumulation in AKO zebrafish. Moreover, Atgl deletion decreased lanosterol synthase (*lss*), which is related to cholesterol synthesis, but enhanced cholesterol utilization genes (*sult2st3*, *hsd3b* and *hsd17b12a*). In addition, several genes involved in phospholipids, especially PE and PC synthesis (*chpt1*, *pcyt1b*, *pmt*, *etnppl* and *etnk2*), were down-regulated in the AKO fish compared with in the WT fish.

The LKO and AKO fish showed different gene expression patterns. In LKO fish, other than the decreased expression of *gpat2* (an enzyme acting on the first step during the synthesis of TAG and phosphoglycerides), genes related to TAG and PL syntheses were not much affected, while lipid catabolism-related genes, such as *lipca*, *acsbg1* and *cpt-1*, were significantly up-regulated. Moreover, the expression of *oxct1b* in LKO fish was upregulated, a key gene that converts ketones to HMG-CoA, indicating increased cholesterol synthesis. However, *hsd3b*, *cyp11a/c* and *cyp17a1* were down-regulated in LKO fish, suggesting weakened synthesis of steroid hormones (derivatives of cholesterol). In short, the transcriptional data coincided with the decreased TAG and increased CE obtained in the LKO zebrafish.

3.4 Autophagy inhibition exacerbated TAG accumulation in liver of AKO fish

To further explore the functions of lipophagy in the absence of Atgl, an inhibitor of autophagy, 3MA, was fed to the AKO fish for 4 weeks. The AKO and AKO+3MA zebrafish showed comparable effects through reduced growth and body protein content, and they accumulated more lipid in the body than occurred in the WT fish (Figure 4A-D). AKO fish had higher TAG content, but not TC, and lower FFA content in the liver than WT fish (Figure 4E-G). However, the AKO+3MA fish had even

higher liver TAG content than AKO fish (Figure 4E). The hepatocytes of AKO and AKO+3MA fish showed LDs that were more numerous and much larger than seen in WT fish (Figure 4I, J), and it was difficult to clearly observe lipophagic process marked by the formation of autophagosomes (AP) and autophagolysosome (APL), which could be found in WT hepatocytes (Figure 4H). Together, these findings indicate that Atgl deficiency induced high fat accumulation, and the additional inhibition of autophagy exacerbated the symptom of fat accumulation in liver, suggesting that lipophagy still plays a role in maintaining physiological homeostasis when lipolysis is depressed in fish liver.

3.5 The Atgl defect inhibited lipolysis without inducing lipophagy in liver

Further assays indicated that the Atgl mutation down-regulated the mRNA and protein contents of *pnpla2* (Atgl) (Figure 5A, C, D, F) as well as the mRNA of most other lipolysis-related genes, including *lipea*, *lipeb*, *mgll*, *fabp10a* and *plin2*. The 3MA supplementation did not alter the expression trend of these genes (Figure 5A). Similarly, the expressions of many autophagy-related genes were reduced in liver of AKO fish, especially *ulk1b*, *beclin1*, *lc3*, *atg4a*, *atg7* and *atg12*. However, 3MA treatment had a compensatory effect by increasing the expressions of some autophagic genes, including *ulk1b*, *beclin1*, *atg5* and *atg12* (Figure 5B). Of note, the Hsl enzyme content (Figure 5E) and P-Hsl protein expression (Figure 5K) were increased in the AKO group compared with in the WT. However, the P-Hsl level was comparable between the AKO and AKO+3MA groups (Figure 5K). The immunofluorescence of Lc3 showed less red fluorescence in the liver of the AKO and AKO+3MA fish (Figure 5G, H). This tendency resembled the protein expression of Lc3-II (Figure 5I), whereas no difference was found in P62 (Figure 5J). These data indicated that the Atgl defect impeded lipolysis and did not cause an obvious compensatory induction of lipophagy in fish liver.

3.6 LKO accumulated TC and the added Atgl inhibition increased LD size in liver

To test the function of lipolysis when lipophagy is blocked, the adult LKO fish were fed a diet with or without supplementation of AI (an Atgl inhibitor) for 4 weeks. Compared with the WT, the LKO and LKO+AI groups displayed similar changes,

with reduced growth, body protein and lipid, but increased visceral mass (Figure 6A-D). In addition, liver TAG content was maintained in the LKO and LKO+AI groups (Figure 6E), while liver TC and LDL-C were increased (Figure 6F-G). Compared with the hepatocytes of WT fish, in which the lipophagy marked by degradation of LDs in lysosomes was easily identified (Figure 6I), hepatocytes of LKO fish had smaller LDs and exhibited far fewer lipophagic characteristics (Figure 6J). However, the size of LDs in liver of LKO+AI fish was generally bigger than that in LKO fish (Figure 6K). Together, these data suggest that Lal was indispensable mainly in cholesterol homeostasis, and that the combined suppression of lipophagy and lipolysis did not affect accumulation of TAG and TC when compared with Lal deficiency.

3.7 Lal deficiency stimulated Atgl expression, and additional Atgl inhibition induced Lal-independent autophagy in liver

As expected, the expression of *lipf* (*lal*) was down-regulated in the LKO fish liver (Figure 7A), and the Lal enzyme content (Figure 7C) and protein expression (Figure 7D, F) were also decreased when compared with the WT fish. Several autophagy-related genes (*tfeb*, *ulk1b*, *beclin1*, *lc3*, *atg4* and *atg7*) had increased as a compensation response in the LKO and LKO+AI groups (Figure 7A), and most lipolysis genes were also up-regulated in liver of LKO fish (Figure 7B), but especially the Atgl content (Figure 7E, F, I). Compared with the WT fish, Lc3-II protein decreased significantly in the liver of LKO fish (Fig. 7F, K), whereas most other autophagy marker proteins, including Beclin1 (Figure 7J) and P62 (Figure 7L), did not differ significantly. Of note, most of these autophagy-related proteins were all up-regulated in the LKO+AI group as compared with the LKO group alone, and the Lc3-IF images also indicated higher Lc3-related red fluorescence in the hepatocytes of the LKO+AI group than seen in cells of the LKO fish (Figure 7G, H). In short, Lal deletion stimulated the expression of Atgl in zebrafish liver, and the combined suppression of Lal and Atgl induced Lal-independent autophagy.

3.8 Simultaneous suppression of lipolysis and lipophagy altered hepatic mitochondrial morphology and exacerbated liver damage

When compared with the AKO fish, the mitochondria obviously increased in number

and size in hepatocytes of AKO+3MA fish (Figure 8A-C), accompanied by higher expressions of genomic mtDNA copy number (nd1 and atp6) and marker genes related to mtDNA proliferation (*ssbp1*) (Figure 8D, E). Moreover, compared with WT fish, genes related to liver damage, such as *il6* and *hspa5*, were increased in the AKO group (Figure 8F) yet did not affect mtDNA (Figure 8D, E). In addition, the expression of genes related to inflammation (*il6*, *il1β* and *tnfα*) and to endoplasmic reticulum (ER) stress (*hspa5*, *xbp1* and *atf6*) were further enhanced in liver of the AKO+3MA fish as compared with the AKO fish (Figure 8F). On the other hand, hepatocytes of specifically the LKO+AI group showed obvious mitochondrial swelling and characteristics of mitophagy, with the common appearance of mitochondria in autophagolysosomal cavities which contained many undegraded LDs (Figure 8G-I). Accordingly, the LKO+AI group had higher expression of lysosomal marker protein (Lamp1) and more obvious co-localization of Lamp1 and Hsp60 than was evident in the WT or LKO groups (Figure 8J, K), suggesting the occurrence of mitophagy. In addition, compared with the WT fish, the atp6 mtDNA copy number was significantly reduced in the LKO fish (Figure 8L), whereas one gene related to mitochondrial proliferation (*tfam*) was increased (Figure 8M). In contrast, the LKO+AI treatment showed a stronger effect than LKO to increase all three mtDNA copy number markers, and two mtDNA proliferation-related genes (*tfam* and *ssbp1*) (Figure 8L, M). Furthermore, nearly all genes related to liver damage, including DNA damage (*ddit3*, *gadd45αa*), apoptosis (*casp3a*, *casp9*), and inflammation (*il6*, *il1β* and *tnfα*), were increased in liver of the LKO and LKO+AI groups, and the LKO+AI group tended to show stronger effects than the LKO fish in the majority of these genes (Figure 8N). Overall, these data indicate that the combined suppression of lipophagy and lipolysis might trigger liver injury and the process of mitophagy.

4. Discussion

To the best of our knowledge, this is the first study to investigate the functions of lipolysis by using a model fish with Atgl deficiency. In the present work, the fish with Atgl deletion showed significant decline in growth, protein loss, OCR reduction and less swimming activity, accompanied by severe TAG accumulation in whole body. Notably, ATGL in mammals has been reported to express predominantly in white and brown adipose tissues, and to a lesser extent in the liver, muscle, heart and small

intestine [7,43], although a few studies indicated that hepatocyte-specific ATGL deletion or overexpression caused hepatic steatosis [8] or ameliorated steatosis [44], respectively. However, previous studies indicated that the *atgl* gene in fish is mainly expressed in the liver and muscle [31,38]. Our study further showed that the AKO fish mainly accumulated numerous, large-sized LDs and high TAG in liver, though no abnormal phenotype was observed in adipose tissue. These results demonstrate that hepatic Atgl is essential for TAG metabolism in zebrafish. This possibly provides an evolutionary reference to understand the roles of Atgl and lipolysis in systemic lipid metabolism.

The TAG lipolysis system comprises of ATGL, HSL and MGL enzymes as a cascade. ATGL is specific for TAG hydrolysis, whereas HSL prefers DG and is able to hydrolyse TAG, MG and CE as well [45]. Therefore, ATGL and HSL are, in theory, complementary. However, the interacting roles of these enzymes during the process of lipolysis in mammals is still debated [6,46,47]. In the present work, the liver of AKO zebrafish down-regulated the expressions of *pnpla2*, *lipeb* and *mgll* as compared with WT fish. However, the Hsl activity and its phosphorylated protein expression (P-Hsl) were slightly elevated in AKO fish liver, suggesting the possibility of its post-transcriptional stimulation. However, the increase of Hsl activity seemed unable to counteract the Atgl deficiency-induced TAG accumulation in the fish. In addition, the increased expression of *abhd5a* (an ATGL co-activator) [48] and the down-regulation of *plin2* (a type of perilipin, whereby its absence facilitates the access of ATGL to LDs) [49] might also be AKO-induced compensatory responses. Nevertheless, the AKO fish had higher expressions of ER stress, apoptosis, and inflammation genes than in the WT, revealing the existence of lipotoxicity [50]. These data emphasize the predominant and essential role of Atgl in lipolysis in zebrafish liver.

The LAL enzyme was thought to be important for lysosomal clearance of LDs, with hydrolytic activities against TAG, CE, and retinyl ester (RE) [51,52]. However, the RE content was too low to be detected in the present study. Similar to mammals [53], Lal deficiency caused CE accumulation and increased cholesterol biosynthesis in zebrafish, suggesting the conserved functions of Lal in vertebrates. In addition to CE, *Lal*$^{-/-}$ mice showed massive accumulation of TAGs in many tissues including liver, spleen, and the small intestine [54]. However, in the present study, surprisingly,

TAG content and total lipid were obviously reduced in the whole body, while hepatic TAG showed almost no difference between the WT and LKO groups of fish. A possible explanation is that, in zebrafish, Lal deletion may stimulate other lipases, such as *atgl* and *lipca* in liver, to maintain lipid homeostasis. In fact, it remains contentious whether LAL-deficient mice accumulate TAG in the liver. For example, in *Liv-Lipa*$^{-/-}$ mice, TAG content was not affected after feeding with a standard chow diet, but when the mice were fed high-fat/high-cholesterol diets (HF/HCD), the accumulation of CE caused severe liver damage and eventually resulted in the reduction of TAG [55]. Moreover, a study noted the existence of a non-LAL acid lipase for TAG, but further identification is needed [56].

Decreased TAG may account for the increased percentages of PE and PC in LKO fish, in agreement with the results of fatty acid composition. Compared with the WT fish, the linoleic acid (n-6 PUFA) was decreased in LKO fish, accompanied by the increased EPA and DHA (n-3 PUFA), suggesting a PUFA remodelling system exists when lipophagy is blocked. Recently, a study using temporal deletion of Atg7 in mice showed that short-term inhibition of autophagy could counteract the decrease of n-3 PUFA caused by feeding with HFD, which also highlighted the role of autophagy in affecting PUFA composition [57]. In the present study, the LKO fish showed aggravated DNA damage, apoptosis and more severe inflammation compared with the AKO fish. The upregulation of *ptgs2b* and *ggt1l2.2* in the LKO fish (Figure 3) possibly facilitated production of pro-inflammatory prostaglandins (PGs) and leukotriene D_4(LTD_4). Accordingly, LAL is regarded as a novel target for the treatment of immunometabolic diseases in mammalian studies [58]. Taken together, our data provide evidence that lipophagy plays a pivotal role in preventing liver damage and maintaining lipid homeostasis in fish.

The relationship between lipolysis and lipophagy is still contested. Here, we found that lipophagy (mainly macrolipophagy) was impaired in the liver of AKO zebrafish, as characterized by the decreased expressions of autophagy-related genes and proteins. Analogously, recent studies in mammals showed that lipolysis and lipophagy partially intersect, wherein ATGL is a common enzyme for both processes [59]. For example, Marttez-Lopez et al. (2016) found that LC3, a well-known marker of the autophagosome, interacts with ATGL at the surface of LDs, and the excision of the LC3-interacting region (LIR) prevented the translocation of ATGL to LDs. In addition,

ATGL was reported to positively regulate autophagic flux and increase the interactions of lysosomes and LC3 with LDs in mammalian hepatocytes [22]. In the present study, lipophagy was not activated in the AKO fish, as evidenced by lower expressions of autophagy-related genes and fewer phagophore-enveloped LDs in the hepatocytes of the AKO fish as compared with in the WT fish. Nevertheless, because the TAG content was increased in the AKO+3MA fish liver when compared with only the AKO liver, we suspect that lipophagy still takes on fundamental roles in degrading TAG when Atgl is blocked. Therefore, it could be concluded that lipophagy might not be activated to compensate for Atgl deletion.

Our results showed the LKO fish stimulated lipolysis, as characterized by decreased body lipid content (mainly pointed to TAG) and high expression of Atgl in the liver. Similarly, the loss of adipose tissue was also found in LAL-deficient mice [19]; nevertheless, the mice lacking LAL in hepatocytes did not stimulate the mRNA expressions of lipolysis-related genes [56]. Although the mechanisms by which lipophagy affects lipolysis are not yet well proven in mammals, our study of zebrafish at least suggests that Atgl-mediated lipolysis can efficiently compensate the deficient effects of Lal on lipid catabolism. However, up-regulated lipolysis cannot compensate for the Lal deficiency-causing liver damage, characterized by highly expressed genes related to DNA damage, apoptosis and inflammation in the liver of LKO fish. A recent study using primary rat hepatocytes found that ATGL preferentially operates on large LDs, whereas the lipophagic machinery mainly targets the small-sized cytoplasmic LDs [60]. Similarly, in the present study, TEM images showed large LDs in the hepatocytes of the AKO fish, and accumulation of small LDs in the hepatocytes of the LKO fish. Our data further indicate that the small hepatic LDs in the LKO fish mainly contained CE instead of TAG, verifying that the function of Lal in cholesterol breakdown is conserved across vertebrates. These data illustrate that lipolysis and lipophagy have different roles in regulating TAG and cholesterol metabolism, respectively. In addition, our study also confirms that the size and lipid composition of LDs may reflect different pathological processes, which would require targeted therapeutic strategies, either in fish or mammals.

Mitochondria are extremely important organelles for cells [61]. However, the morphological and functional changes of mitochondria during the inhibition of lipolysis and/or lipophagy have not been well explored. In the present study, the

morphological characteristics of mitochondria in the hepatocytes of AKO fish were comparable to those of WT fish, as well as the mtDNA copy number and associated gene expression. However, *Atgl*$^{-/-}$ mice accumulated LDs in the liver with intact mitochondria surrounded by rough ER [62]. The Lal deficiency in the present study caused more severe mitochondrial damage as compared with outcomes for the AKO fish. This was verified by decreased expression of mt-*atp6* and weaker green fluorescence of Hsp60. Of note, mice with Niemann–Pick type C (NPC) mutant characterized by high cholesterol accumulation in endosomes and lysosomes, particularly in mitochondrial membranes, showed markedly decreased mitochondrial membrane potential (MMP) and diminished ATP production [63]. This indicates a possible correlation between cellular cholesterol accumulation and mitochondrial damage. Therefore, Lal deficiency might impair the integrity of mitochondrial membrane structures by changing the cellular lipid profile, consequently causing mitochondrial dysfunction.

So far, little is known about changes in mitochondria when lipolysis and lipophagy are simultaneously suppressed. Our data suggest that when the AKO fish were treated with additional 3MA, mitochondrial swelling increased, and the mitochondria were obviously surrounded by rough ER. This phenomenon was supported by the up-regulation of genes related to ER-stress (*hspa5*, *xbp1* and *atf6*), mtDNA synthesis (*ssbp1*), and mtDNA copy number (mt-*nd1* and mt-*atp6*). Mitochondrial damage seemed to be more severe when AI was administered to the LKO fish as compared with the AKO+3MA fish, because of the potential occurrence of mitophagy, including the formation of mitochondria-containing autophagosomes, their fusion to lysosomes, and the digestion of dysfunctional mitochondria. In addition, the immunofluorescence co-localization of Lamp1 and Hsp60 as well as high expressions of autophagy related proteins (Lc3, Beclin1 and P62) also suggested mitophagy in the livers of LKO+AI fish. Importantly, AI is a specific inhibitor of Atgl, while 3MA mainly depresses autophagy through inhibition of class III PI3K [64], but not Lal. Therefore, 3MA might also inhibit mitophagy, which would explain why the AKO+3MA treatment was less effective in inducing potential mitophagy than the LKO+AI treatment.

In short, our data show that when the two intracellular LD degrading pathways are blocked synchronously, the removal of damaged mitochondria through mitophagy

may be a protective cellular strategy to prevent cell death. On the other hand, when lipolysis and lipophagy are both blocked, the increased mitophagy may also be an alternative process to supply energy. This interaction among cellular organelles under lipid-sourced energy exhaustion merits further investigation.

5. Conclusions

The results of the present study suggest that lipolysis and lipophagy are each important to maintain lipid metabolism homeostasis across vertebrates. The absence of Atgl or Lal in zebrafish caused retard growth, sluggish movement, and reduced OCR. As summarized in Figure 9, Atgl-mediated lipolysis showed a stronger potential to degrade large-sized LDs enriched with TAG, and lipolysis dysfunction did not stimulate lipophagy to counteract the TAG accumulation. Lipophagy broke down mainly small LDs, which contained high cholesterol esters, and Lal deficiency induced compensatory lipolysis but caused severe cellular damage. The simultaneous suppression of lipolysis and lipophagy may possibly trigger mitophagy. Overall, the present study provides a reference for better understanding both the separate and interactive roles of lipolysis and lipophagy from the aspect of neutral and acidic lipases in zebrafish. Finally, this study provides insights for interpreting lipid homeostasis from an evolutionary or comparative physiological point of view.

Acknowledgments

This work was financed by the National Natural Science Fund of China (31830102) and Program of Shanghai Academic Research Leader (19XD1421200). We thank Mark Cleasby, PhD, from Liwen Bianji, Edanz Group China (www.liwenbianji.cn/ac), for editing the English text of a draft of this manuscript.

Authors contribution

ZY. D. and SL. H. conceived the study and designed the experiments. SL. H. and YC. Q. carried out the experiments, analysed the data and wrote the manuscript. J. W., LQ. C. and ML. Z. contributed reagents/materials/analysis tools. SL. H. S. M. L. and ZY. D. wrote and revised the manuscript. All authors read and approved the final manuscript.

Compliance with ethics guidelines

All authors declare that they have no conflict of interest or financial conflicts to disclose.

Conflict of interest

We declare that we have no financial and personal relationships with other people or organizations that can inappropriately influence our work. There is no professional or other personal interest of any nature or kind in any product, service and/or company that could be construed as influencing the position presented in, or the review of, the manuscript.

References

[1] Hashemi HF, Goodman JM. The life cycle of lipid droplets. Curr Opin Cell Biol. 2015;33:119-124.

[2] Pol A, Gross SP, Parton RG. Biogenesis of the multifunctional lipid droplet: Lipids, proteins, and sites. J Cell Biol. 2014;204(5):635-646.

[3] Welte MA, Gould AP. Lipid droplet functions beyond energy storage. Biochim Biophys Acta Mol Cell Biol Lipids. 2017;1862(10):1260-1272.

[4] Olzmann JA, Carvalho P. Dynamics and functions of lipid droplets. Nat Rev Mol Cell Biol. 2019;20(3):137-155.

[5] Lass A, Zimmermann R, Oberer M, et al. Lipolysis–a highly regulated multi-enzyme complex mediates the catabolism of cellular fat stores. Prog Lipid Res. 2011;50(1):14-27.

[6] Haemmerle G, Lass A, Zimmermann R, et al. Defective lipolysis and altered energy metabolism in mice lacking adipose triglyceride lipase. Science. 2006;312(5774):734-737.

[7] Zimmermann R, Strauss JG, Haemmerle G, et al. Fat mobilization in adipose tissue is promoted by adipose triglyceride lipase. Science. 2004;306(5700):1383-1386.

Journal Pre-proof

630 [8] Wu JW, Wang SP, Alvarez F, et al. Deficiency of liver adipose triglyceride lipase in mice
631 causes progressive hepatic steatosis. Hepatology. 2011;54(1):122-132.
632 [9] Fischer J, Lefevre C, Morava E, et al. The gene encoding adipose triglyceride lipase
633 (PNPLA2) is mutated in neutral lipid storage disease with myopathy. Nat Genet.
634 2007;39(1):28-30.
635 [10] Missaglia S, Tasca E, Angelini C, et al. Novel missense mutations in PNPLA2 causing late
636 onset and clinical heterogeneity of neutral lipid storage disease with myopathy in three
637 siblings. Mol Genet Metab. 2015;115(2):110-117.
638 [11] Massa R, Pozzessere S, Rastelli E, et al. Neutral lipid storage disease with myopathy and
639 extended phenotype with novel PNPLA2 mutation. Muscle Nerve. 2016;53(4):644-648.
640 [12] Hoy AJ, Bruce CR, Turpin SM, et al. Adipose triglyceride lipase-null mice are resistant to
641 high-fat diet–induced insulin resistance despite reduced energy expenditure and ectopic
642 lipid accumulation. Endocrinology. 2011;152(1):48-58.
643 [13] Singh R, Kaushik S, Wang YJ, et al. Autophagy regulates lipid metabolism. Nature.
644 2009;458(6):1131-1135.
645 [14] Wagner C, Hois V, Pajed L, et al. Lysosomal acid lipase is the major acid retinyl ester
646 hydrolase in cultured human hepatic stellate cells but not essential for retinyl ester
647 degradation. Biochim Biophys Acta Mol Cell Biol Lipids. 2020;1865:158730.
648 [15] Zechner R, Madeo F, Kratky D. Cytosolic lipolysis and lipophagy: two sides of the same
649 coin. Nat Rev Mol Cell Biol. 2017;18(11):671-684.
650 [16] Zechner R, Zimmermann R, Eichmann TO, et al. FAT SIGNALS-lipases and lipolysis in
651 lipid metabolism and signaling. Cell Metab. 2012;15(3):279-291.

652 [17] Strebinger G, Muller E, Feldman A, et al. Lysosomal acid lipase deficiency – early
653 diagnosis is the key. Hepat Med. 2019;11:79-88.
654 [18] Reiner Ž, Guardamagna O, Nair D, et al. Lysosomal acid lipase deficiency – An
655 under-recognized cause of dyslipidaemia and liver dysfunction. Atherosclerosis.
656 2014;235(1):21-30.
657 [19] Du H, Heur M, Duanmu M, et al. Lysosomal acid lipase-deficient mice: depletion of white
658 and brown fat, severe hepatosplenomegaly, and shortened life span. J Lipid Res.
659 2001;42(4):489-500.
660 [20] Radovic B, Vujic N, Leopold C, et al. Lysosomal acid lipase regulates VLDL synthesis and
661 insulin sensitivity in mice. Diabetologia. 2016;59(8):1743-1752.
662 [21] Martinez-Lopez N, Garcia-Macia M, Sahu S, et al. Autophagy in the CNS and periphery
663 coordinate lipophagy and lipolysis in the brown adipose tissue and liver. Cell Metab.
664 2016;23(1):113-127.
665 [22] Sathyanarayan A, Mashek MT, Mashek DG. ATGL promotes autophagy/lipophagy via
666 SIRT1 to control hepatic lipid droplet catabolism. Cell Rep. 2017;19(1):1-9.
667 [23] Goeritzer M, Vujic N, Schlager S, et al. Active autophagy but not lipophagy in
668 macrophages with defective lipolysis. Biochim Biophys Acta Mol Cell Biol Lipids.
669 2015;1851(10):1304-1316.
670 [24] Dupont N, Chauhan S, Arko-Mensah J, et al. Neutral lipid stores and lipase PNPLA5
671 contribute to autophagosome biogenesis. Curr Biol. 2014;24(6):609-620.
672 [25] Khan SA, Sathyanarayan A, Mashek MT, et al. ATGL-catalyzed lipolysis regulates SIRT1
673 to control PGC-1α/PPAR-α signaling. Diabetes. 2015;64(2):418-426.

674 [26] Schulze RJ, Sathyanarayan A, Mashek DG. Breaking fat: The regulation and mechanisms
675 of lipophagy ☆. Biochim Biophys Acta Mol Cell Biol Lipids. 2017;1862(10 Pt
676 B):S1388198117301129.
677 [27] Deng K, Pan M, Liu J, et al. Chronic stress of high dietary carbohydrate level causes
678 inflammation and influences glucose transport through SOCS3 in Japanese flounder
679 Paralichthys olivaceus. Sci Rep. 2018;8(1):1-13.
680 [28] Wang X, Li Y, Hou C, et al. Physiological and molecular changes in large yellow croaker
681 (*P seudosciaena crocea R.*) with high-fat diet-induced fatty liver disease. Aquac Res.
682 2015;46(2):272-282.
683 [29] Wang J, Liu Y, Tian L, et al. Effect of dietary lipid level on growth performance, lipid
684 deposition, hepatic lipogenesis in juvenile cobia (*Rachycentron canadum*). Aquaculture.
685 2005;249(249):439-447.
686 [30] Liu D, Mai K, Ai Q. Tumor necrosis factor alpha is a potent regulator in fish adipose tissue.
687 Aquaculture. 2015;436:63-71.
688 [31] Sun J, Ji H, Li X-X, et al. Lipolytic enzymes involving lipolysis in Teleost: Synteny,
689 structure, tissue distribution, and expression in grass carp (*Ctenopharyngodon idella*).
690 Comp Biochem Physiol B, Biochem Mol Biol. 2016;198:110-118.
691 [32] Wang X, Wang Y, Li Y. Adipose triglyceride lipase (ATGL) clone, expression pattern, and
692 regulation by different lipid sources and lipid levels in large yellow croaker
693 (*Pseudosciaena crocea R.*). Mar Biotechnol. 2013;15(2):197-205.
694 [33] Han SL, Liu Y, Limbu SM, et al. The reduction of lipid-sourced energy production caused
695 by ATGL inhibition cannot be compensated by activation of HSL, autophagy, and

696 utilization of other nutrients in fish. Fish Physiol Biochem. 2020;47(1):173-188.

697 [34] Wang J, Han SL, Lu DL, et al. Inhibited lipophagy suppresses lipid metabolism in

698 zebrafish liver cells. Front Physiol. 2019;10:1077.

699 [35] Wang J, Han SL, Li LY, et al. Lipophagy is essential for lipid metabolism in fish. Sci Bull.

700 2018;63(14):879-882.

701 [36] Han SL, Wang J, Zhang YX, et al. Inhibited autophagy impairs systemic nutrient

702 metabolism in Nile tilapia. Comp Biochem Physiol Part A Mol Integr Physiol.

703 2019;236:110521.

704 [37] Mawed SA, He Y, Zhang J, et al. Strategy of hepatic metabolic defects induced by beclin1

705 heterozygosity in adult zebrafish. Int J Mol Sci. 2020;21(4):1533.

706 [38] Dai YJ, Liu WB, Li XF, et al. Molecular cloning of adipose triglyceride lipase (ATGL) gene

707 from blunt snout bream and its expression after LPS-induced TNF-α factor. Fish physiol

708 Biochem. 2018;44(4):1143-1157.

709 [39] Lu D, Ma Q, Wang J, et al. Fasting enhances cold resistance in fish through stimulating

710 lipid catabolism and autophagy. J Physiol. 2019;597(6):1585-1603.

711 [40] Li LY, Lv HB, Jiang ZY, et al. Peroxisomal proliferator-activated receptor α-b deficiency

712 induces the reprogramming of nutrient metabolism in zebrafish. J Physiol.

713 2020;598(20):4537-4553.

714 [41] Liu Y, Wen J, Ning L, et al. Comparison of effects of dietary-specific fatty acids on growth

715 and lipid metabolism in Nile tilapia. Aquac Nutr. 2019;25(4):862-872.

716 [42] Limbu SM, Zhou L, Sun S-X, et al. Chronic exposure to low environmental concentrations

717 and legal aquaculture doses of antibiotics cause systemic adverse effects in Nile tilapia

718 and provoke differential human health risk. Environ Int. 2018;115:205-219.

719 [43] Obrowsky S, Chandak PG, Patankar JV, et al. Adipose triglyceride lipase is a TG
720 hydrolase of the small intestine and regulates intestinal PPARα signaling. J Lipid Res.
721 2013;54(2):425-435.

722 [44] Reid BN, Ables GP, Otlivanchik OA, et al. Hepatic overexpression of hormone-sensitive
723 lipase and adipose triglyceride lipase promotes fatty acid oxidation, stimulates direct
724 release of free fatty acids, and ameliorates steatosis. J Biol Chem.
725 2008;283(19):13087-13099.

726 [45] Lafontan M, Langin D. Lipolysis and lipid mobilization in human adipose tissue. Prog Lipid
727 Res. 2009;48(5):275-297.

728 [46] Jiang WW, Wang SP, Casavant S, et al. Fasting energy homeostasis in mice with adipose
729 deficiency of desnutrin/adipose triglyceride lipase. Endocrinology.
730 2012;153(5):2198-2207.

731 [47] Zhang X, Zhang CC, Yang H, et al. An epistatic interaction between pnpla2 and lipe
732 reveals new pathways of adipose tissue lipolysis. Cells. 2019;8(5):395.

733 [48] Korbelius M, Vujic N, Sachdev V, et al. ATGL/CGI-58-dependent hydrolysis of a lipid
734 storage pool in murine enterocytes. Cell Rep. 2019;28(7):1923-1934. e1924.

735 [49] Bell M, Wang H, Chen H, et al. Consequences of lipid droplet coat protein downregulation
736 in liver cells: abnormal lipid droplet metabolism and induction of insulin resistance.
737 Diabetes. 2008;57(8):2037-2045.

738 [50] Han J, Kaufman RJ. The role of ER stress in lipid metabolism and lipotoxicity. J Lipid Res.
739 2016;57(8):1329-1338.

740 [51] Grumet L, Eichmann TO, Taschler U, et al. Lysosomal acid lipase hydrolyzes retinyl ester
741 and affects retinoid turnover. J Biol Chem. 2016;291(34):17977-17987.
742 [52] Du H, Duanmu M, Witte DP, et al. Targeted disruption of the mouse lysosomal acid lipase
743 gene: long-term survival with massive cholesteryl ester and triglyceride storage. Hum Mol
744 Genet. 1998;7(9):1347-1354.
745 [53] Aqul A, Lopez AM, Posey KS, et al. Hepatic entrapment of esterified cholesterol drives
746 continual expansion of whole body sterol pool in lysosomal acid lipase-deficient mice. Am
747 J Physiol Gastrointest Liver Physiol. 2014;307(8):G836-G847.
748 [54] Li F, Zhang H. Lysosomal acid lipase in lipid metabolism and beyond. Arterioscler Thromb
749 Vasc Biol. 2019;39(5):850-856.
750 [55] Leopold C, Duta-Mare M, Sachdev V, et al. Hepatocyte-specific lysosomal acid lipase
751 deficiency protects mice from diet-induced obesity but promotes hepatic inflammation.
752 Biochim Biophys Acta Mol Cell Biol Lipids. 2019;1864(4):500-511.
753 [56] Pajed L, Wagner C, Taschler U, et al. Hepatocyte-specific deletion of lysosomal acid
754 lipase leads to cholesteryl ester but not triglyceride or retinyl ester accumulation. J Biol
755 Chem. 2019;294(25):9118-9133.
756 [57] Chu KY, Mellet N, Meikle PJ, et al. Short-term inhibition of autophagy benefits pancreatic
757 β-cells by augmenting ether lipids and peroxisomal function, and by countering depletion
758 of n-3 polyunsaturated fatty acids after fat-feeding. Mol Metab. 2020;40:101023.
759 [58] Gomaraschi M, Bonacina F, Norata G. Lysosomal acid lipase: from cellular lipid handler to
760 immunometabolic target. Trends Pharmacol Sci. 2019;40(2):104-115.
761 [59] Missaglia S, Coleman RA, Mordente A, et al. Neutral lipid storage diseases as cellular

762 model to study lipid droplet function. Cells. 2019;8(2):187.

763 [60] Schott MB, Weller SG, Schulze RJ, et al. Lipid droplet size directs lipolysis and lipophagy

764 catabolism in hepatocytes. J Cell Biol. 2019;218(10):3320-3335.

765 [61] Simões IC, Fontes A, Pinton P, et al. Mitochondria in non-alcoholic fatty liver disease. Int J

766 Biochem Cell Biol. 2018;95:93-99.

767 [62] Kratky D, Obrowsky S, Kolb D, et al. Pleiotropic regulation of mitochondrial function by

768 adipose triglyceride lipase-mediated lipolysis. Biochimie. 2014;96.106-112.

769 [63] De la Mata M, Cotán D, Villanueva-Paz M, et al. Mitochondrial dysfunction in lysosomal

770 storage disorders. Diseases. 2016;4(4):31.

771 [64] Mathai BJ, Meijer AH, Simonsen A. Studying autophagy in zebrafish. Cells.

772 2017;6(3):21.

773

774

775 **Figure 1. The general phenotypes of *atgl*$^{-/-}$ (AKO) zebrafish.** (A) the zebrafish
776 *pnpla2* (atgl) target site, the deduced peptide length of WT, *pnpla2*$^{-/-}$ and the DNA
777 sequencing results of homozygous mutant; (B) growth curve of juvenile fish; (C)
778 locomotor activity (n = 6); (D) oxygen consumption rate (OCR) of WT and *atgl*$^{-/-}$ fish
779 (n = 30), OCR = [ΔO2 concentration (mg /L) × water volume (L)] / [body weight (g)
780 × time (h)]; (E) whole fish protein (n = 6); (F) whole fish total lipid (n = 6); (G)
781 viscera somatic index (VSI) = visceral mass × 100%/fish weight (n = 6); (H) TAG
782 content in whole fish (n = 6); (I) phospholipid (PL) content in whole fish (n = 6); (J)
783 lipid class measured by TLC (average value, n = 4); (K) fatty acid composition
784 detected by GC (n = 4); (L) visceral anatomy of WT, *atgl*$^{-/-}$ fish; H & E staining of
785 liver from WT, *atgl*$^{-/-}$fish, scale bars, 50 μm. Data represent mean ± SEM. Statistical
786 significance was determined by two-tailed independent *t*-test ($p < 0.05$).
787

788 **Figure 2. The general phenotypes of *lal*$^{-/-}$ (LKO) zebrafish.** (A) the zebrafish *lipf*
789 (lal) target site, the deduced peptide length of WT, *lipf*$^{-/-}$ and the DNA sequencing
790 results of homozygous mutant; (B) growth curve of juvenile fish; (C) locomotor
791 activity (n = 6); (D) OCR of WT and *lal*$^{-/-}$ fish (n = 30); (E) VSI (n = 6); (F) whole
792 fish protein (n = 6); (G) whole fish total lipid (n = 6); (H) TAG content in whole fish
793 (n = 6); (I) phospholipid (PL) content in whole fish (n = 6); (J) lipid class measured

by TLC (average value, n = 4); (K) fatty acid composition detected by GC (n = 4); (L) visceral anatomy of WT, *lal*$^{-/-}$ fish; H&E staining of liver from WT, *lal*$^{-/-}$ fish, scale bars, 50 μm. Data represent mean ± SEM. Statistical significance was determined by two-tailed independent *t*-test ($p < 0.05$).

Figure 3. Transcriptional regulation of AKO and LKO in lipid metabolism. *gpat2*, glycerol-3-phosphate acyltransferase 2, mitochondrial; *dgat2*, diacylglycerol O-acyltransferase 2; *lipca*, lipase, hepatic a; *mogat3a*, monoacylglycerol O-acyltransferase 3a; *fads2*, fatty acid desaturase 2; *elovl2*, ELOVL fatty acid elongase 2; *elovl7b*, ELOVL fatty acid elongase 7b; *acsl3a*, acyl-CoA synthetase long chain family member 3a; *acsbg1*, acyl-CoA synthetase bubblegum family member 1; *ehhadh*, enoyl-CoA, hydratase/3-hydroxyacyl CoA dehydrogenase; *acaa1/2*, acetyl-CoA acyltransferase 1/2; *cpt-1*(Gene ID: 100333227), carnitine O-palmitoyltransferase 1, liver isoform-like; *oxct1b*, 3-oxoacid CoA transferase 1b; *lss*, lanosterol synthase (2,3-oxidosqualene-lanosterolcyclase); *lipg*, lipase, endothelial; *sult2st3*, sulfotransferase family 2, cytosolicsulfotransferase 3; *cyp7a1*, cytochrome P450, family 7, subfamily A, polypeptide1; *hsd3b*, hydroxy-delta-5-steroid dehydrogenase, 3 beta-andsteroid delta-isomerase; *hsd17b12a*, hydroxysteroid (17-beta) dehydrogenase 12a; *cyp11a/c*, cytochrome P450, family 11, subfamily A/C, polypeptide 1; *cyp17a1*, cytochrome P450, family 17, subfamily A, polypeptide 1; *enpp6*, ectonucleotide pyrophosphatase/phosphodiesterase 6; *pla2g*, phospholipase A2, group XIIB/XIIA /III; *ptgs2b*, prostaglandin-endoperoxide synthase 2b; *ptgdsb.1*, prostaglandin D2 synthase b, tandem duplicate 1; *lta4h*, leukotriene A4 hydrolase; *ggt1l2.2*, gamma-glutamyltransferase 1 like 2.2; *chpt1*, choline phosphotransferase 1; *pcyt1b*, phosphate cytidylyltransferase 1, choline, beta b; *pmt*, phosphoethanolamine methyltransferase; *etnppl*, ethanolamine-phosphate phospho-lyase; *etnk2*, ethanolamine kinase 2; *phosphol1*, phosphatase, orphan 1; *acer1*, alkaline ceramidase 1; *sphk1*, sphingosine kinase 1. The summary table about TAG/Chol/PE directionality is based on the qualitative impressions of pathway analysis, which can help to interpret the diagram drew above.

Figure 4. The lipid deposition in the liver of AKO zebrafish with or without 3MA treatment. (A-D) data from WT, *atgl*$^{-/-}$ and *atgl*$^{-/-}$+3MA three groups, (A) growth curve; (B) VSI; (C) whole fish protein; (D) whole fish total lipid; (E) triacylglycerols (TAG) content in the liver (n = 6); (F) total cholesterol including cholesteryl ester and free cholesterol in liver (n = 6); (G) free fatty acid in liver (n = 6); (H-J) transmission electron microscope (TEM) images of the liver from WT, *atgl*$^{-/-}$ and *atgl*$^{-/-}$ + 3MA group respectively, LDs: lipid droplets, M: mitochondria, N: nucleus, L: lysosome, ER: endoplasmic reticulum, AP: autophagosome, APL: autophagolysosomes. Statistical significance was determined by one-way ANOVA ($p < 0.05$).

Figure 5. The lipolysis and autophagy related indexes in the liver of AKO zebrafish with or without 3MA treatment. (A) the expression of lipolysis related genes in fish liver (n = 6); (B) the expression of autophagy related genes in fish liver

(n = 6); (C) the content of Atgl enzyme in fish liver measured by ELISA kit (n = 6); (D) densitometry quantification of the Atgl immunoblots (n = 3); (E) the content of Hsl enzyme in fish liver measured by ELISA kit (n = 6); (F) western blot analysis of lipolysis and autophagy related proteins in liver; (G) the immunofluorescence (IF) of Lc3 in liver sections, scale bars, 50 μm; (H) quantification of the tissue IF (n = 3); (I-L) densitometry quantification of the immunoblots (n = 3). Data represent mean ± SEM. Statistical significance was determined by one-way ANOVA ($p < 0.05$).

Figure 6. **The lipid deposition in the liver of LKO zebrafish with or without AI treatment.** (A-D) data from WT, *lal*$^{-/-}$ and *lal*$^{-/-}$+AI three groups, (A) growth curve; (B) VSI; (C) whole fish protein; (D) whole fish total lipid; (E) TAG content in liver (n = 6); (F) total cholesterol in liver (n = 6); (G) low density lipoprotein cholesterol (LDL-C) in liver (n = 6); (H) free fatty acid in liver (n = 6); (I-K) TEM photographs of the liver from WT, *lal*$^{-/-}$ and *lal*$^{-/-}$ + AI group respectively, LDs: lipid droplets, M: mitochondria, N: nucleus, L: lysosome, ER: endoplasmic reticulum, AP: autophagosome, APL: autophagolysosomes. Statistical significance was determined by one-way ANOVA ($p < 0.05$).

Figure 7. The autophagy and lipolysis related indexes measured in liver of LKO zebrafish with or without AI treatment. (A) the expression of autophagy related genes in fish liver (n = 6); (B) the expression of lipolysis related genes in fish liver (n = 6); (C) the content of Lal enzyme in fish liver measured by ELISA kit (n = 6); (D) densitometry quantification of the Lal immunoblots (n = 3); (E) the content of Atgl enzyme in liver measured by ELISA kit (n = 6); (F) western blot analysis of lipolysis and autophagy related proteins in liver (n = 3); (G) the immunofluorescence (IF) of Lc3 in liver sections, scale bars, 50 μm; (H) quantification of the tissue IF (n = 3); (I-L) densitometry quantification of the immunoblots (n = 3). Data represent mean ± SEM. Statistical significance was determined by one-way ANOVA ($p < 0.05$).

Figure 8. The mitochondrial characteristics and cell damages in the liver of zebrafish with simultaneously deficient lipolysis and lipophagy. (A) TEM photographs of liver from *atgl*$^{-/-}$ + 3MA group; (B) mitochondria number per hepatic cell from WT, *atgl*$^{-/-}$ and *atgl*$^{-/-}$+3MA groups (n=6); (C) distribution of mitochondrial length (the longest diameter) for all mitochondria (＞135) in every group; (D) quantification of liver mtDNA copy number by qPCR analysis (n = 6); (E) the expression of mtDNA synthesis related genes in the liver (n = 6); (F) the expression of liver damage related genes (n = 6); (G) TEM photographs of liver from *lal*$^{-/-}$ + AI group; (H) mitochondria number per hepatic cell from WT, *lal*$^{-/-}$ and *lal*$^{-/-}$+AI groups (n=6); (I) distribution of mitochondrial length (the longest diameter) for all mitochondria (＞135) in every group; (J) the IF- colocalization of Lamp1 (red) and Hsp60 (green) in liver sections, scale bars, 50 μm; (K) quantification of the average fluorescent intensity (n = 3); (L) quantification of liver mtDNA copy number by qPCR analysis (n = 6); (M) the expression of mtDNA synthesis related genes in liver (n = 6); (N) the expression of liver damage related genes (n = 6). Statistical

882 significance was determined by one-way ANOVA ($p < 0.05$).

883

884 **Figure 9. The proposed individual and interactive roles of lipolysis and lipophagy**
885 **in zebrafish.** Atgl-mediated lipolysis has a stronger effect to degrade large LDs
886 enriched with TAG and lipolysis dysfunction fail to stimulate lipophagy. However,
887 lipophagy mainly breaks down small LDs, which contain high cholesterol esters and
888 Lal deficiency induces compensatory lipolysis but causes severe cellular damage. The
889 simultaneous suppression of lipolysis and lipophagy may trigger mitophagy to supply
890 energy.
891

Journal Pre-proof

Highlights

- Atgl or Lal mutation causes different lipid metabolism patterns;
- Lipolysis and lipophagy have different preferences for substrate selection;
- Lipolysis and lipophagy are not necessarily substitutional in fish liver;
- Mitochondrial form is changed when lipolysis and lipophagy are both suppressed.

Journal Pre-proof

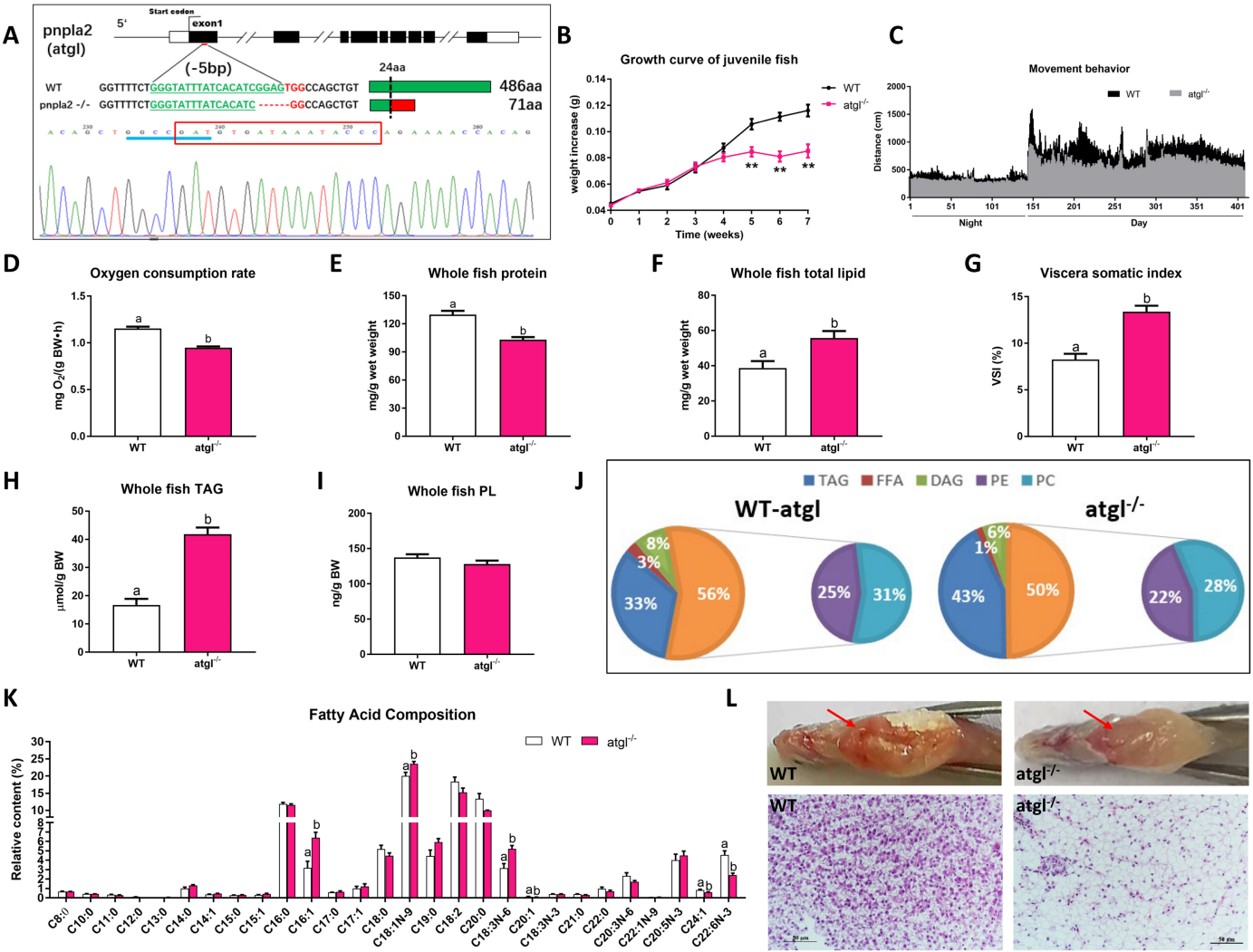

A
pnpla2
(atgl)
Start codon
5'
exon1
(-5bp)
24aa
WT
GGTTTTCTGGGTATTTATCACATCGGAGTGGCCAGCTGT
486aa
pnpla2 -/-
GGTTTTCTGGGTATTTATCACATC------GGCCAGCTGT
71aa
B
Growth curve of juvenile fish
weight increase (g)
Time (weeks)
WT
atgl-/-
C
Movement behavior
Distance (cm)
Night
Day
D
Oxygen consumption rate
mg O2/(g BW•h)
E
Whole fish protein
mg/g wet weight
F
Whole fish total lipid
mg/g wet weight
G
Viscera somatic index
VSI (%)
H
Whole fish TAG
μmol/g BW
I
Whole fish PL
ng/g BW
J
TAG
FFA
DAG
PE
PC
WT-atgl
atgl-/-
8%
3%
56%
33%
25%
31%
6%
1%
50%
43%
22%
28%
K
Fatty Acid Composition
Relative content (%)
C8:0
C10:0
C11:0
C12:0
C13:0
C14:0
C14:1
C15:0
C15:1
C16:0
C16:1
C17:0
C17:1
C18:0
C18:1N-9
C19:0
C18:2
C20:0
C18:3N-6
C20:1
C18:3N-3
C21:0
C22:0
C20:3N-6
C22:1N-9
C20:5N-3
C24:1
C22:6N-3
L
WT
atgl-/-
WT
atgl-/-

Figure 1

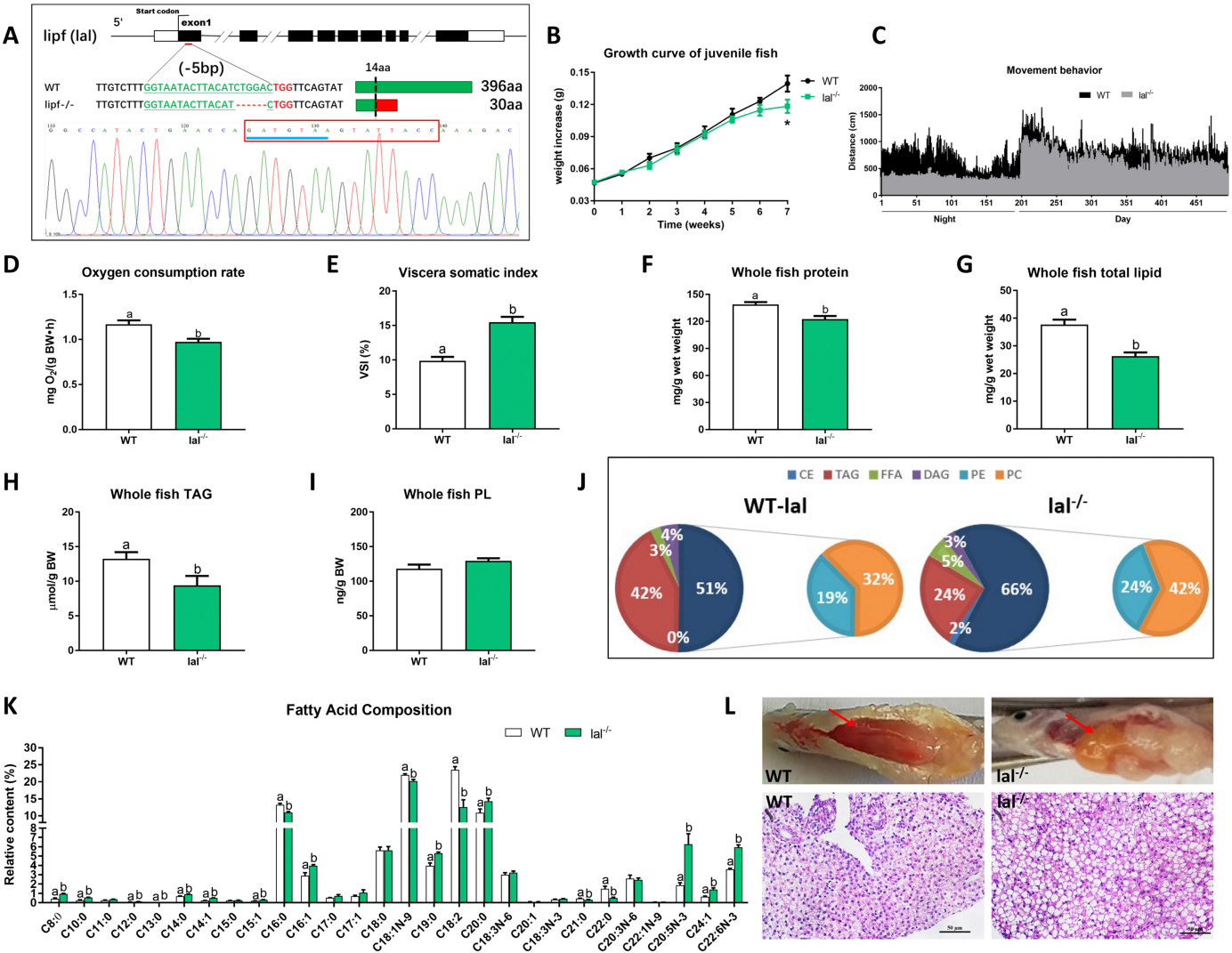
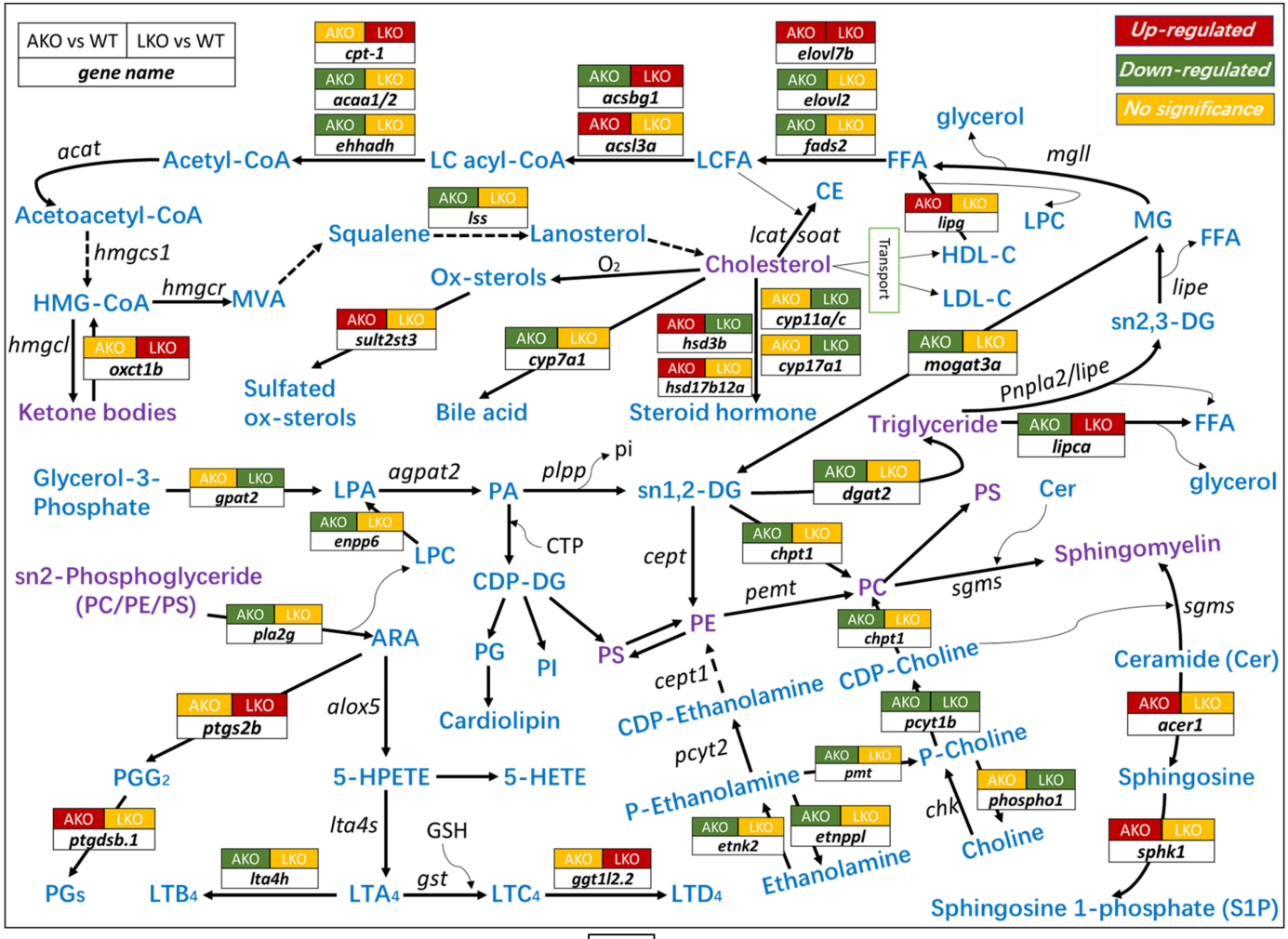

A
lipf (lal)
Start codon
5'
exon1
(-5bp)
14aa
WT TTGTCTTTGGTAATACTTACATCTGGACTGGTTCAGTAT 396aa
lipf-/- TTGTCTTTGGTAATACTTACAT------CTGGTTCAGTAT 30aa
B
Growth curve of juvenile fish
weight increase (g)
Time (weeks)
WT
lal-/-
C
Movement behavior
Distance (cm)
Night
Day
D
Oxygen consumption rate
mg O2/(g BW•h)
E
Viscera somatic index
VSI (%)
F
Whole fish protein
mg/g wet weight
G
Whole fish total lipid
mg/g wet weight
H
Whole fish TAG
μmol/g BW
I
Whole fish PL
ng/g BW
J
CE TAG FFA DAG PE PC
WT-lal
lal-/-
51%
42%
4%
3%
0%
32%
19%
66%
24%
3%
5%
2%
42%
K
Fatty Acid Composition
Relative content (%)
C8:0 C10:0 C11:0 C12:0 C13:0 C14:0 C14:1 C15:0 C15:1 C16:0 C16:1 C17:0 C17:1 C18:0 C18:1N-9 C19:0 C18:2 C20:0 C18:3N-6 C20:1 C18:3N-3 C21:0 C22:0 C20:3N-6 C22:1N-9 C20:5N-3 C24:1 C22:6N-3
L
WT
lal-/-
WT
lal-/-

Figure 2



Group	TAG synthesis	TAG catabolism	Chol synthesis	Chol utilization	PE/PC synthesis
AKO vs WT	↓↓	↓↓	↓	↑	↓↓
LKO vs WT	—	↑	↑	↓↓	—

Figure 3

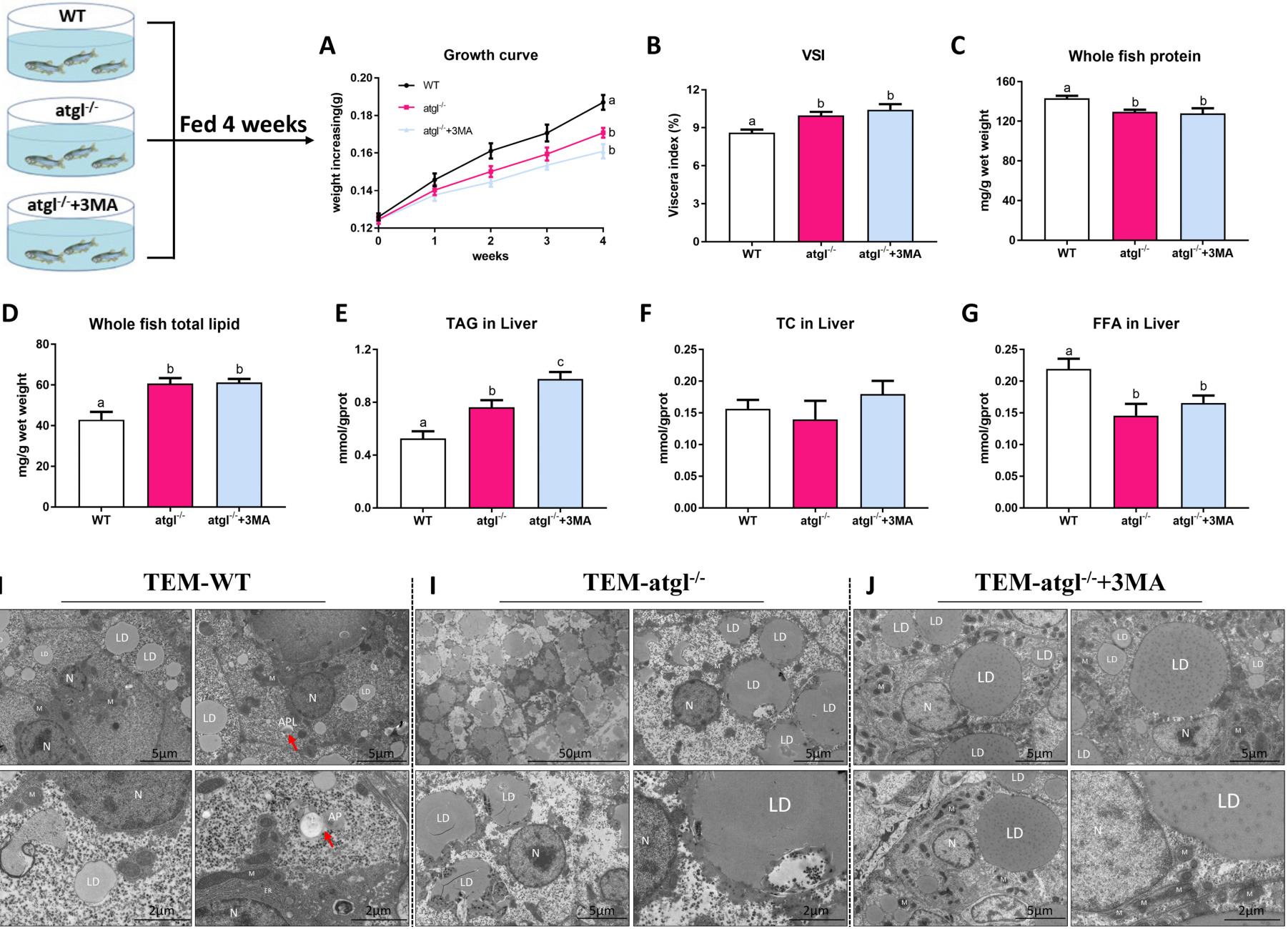

WT
atgl-/-
atgl-/-+3MA
Fed 4 weeks
A
Growth curve
weight increasing(g)
weeks
WT
atgl-/-
atgl-/-+3MA
B
VSI
Viscera index (%)
C
Whole fish protein
mg/g wet weight
D
Whole fish total lipid
mg/g wet weight
E
TAG in Liver
mmol/gprot
F
TC in Liver
mmol/gprot
G
FFA in Liver
mmol/gprot
H
TEM-WT
I
TEM-atgl-/-
J
TEM-atgl-/-+3MA
LD
N
M
APL
AP
ER
5μm
50μm
2μm

Figure 4

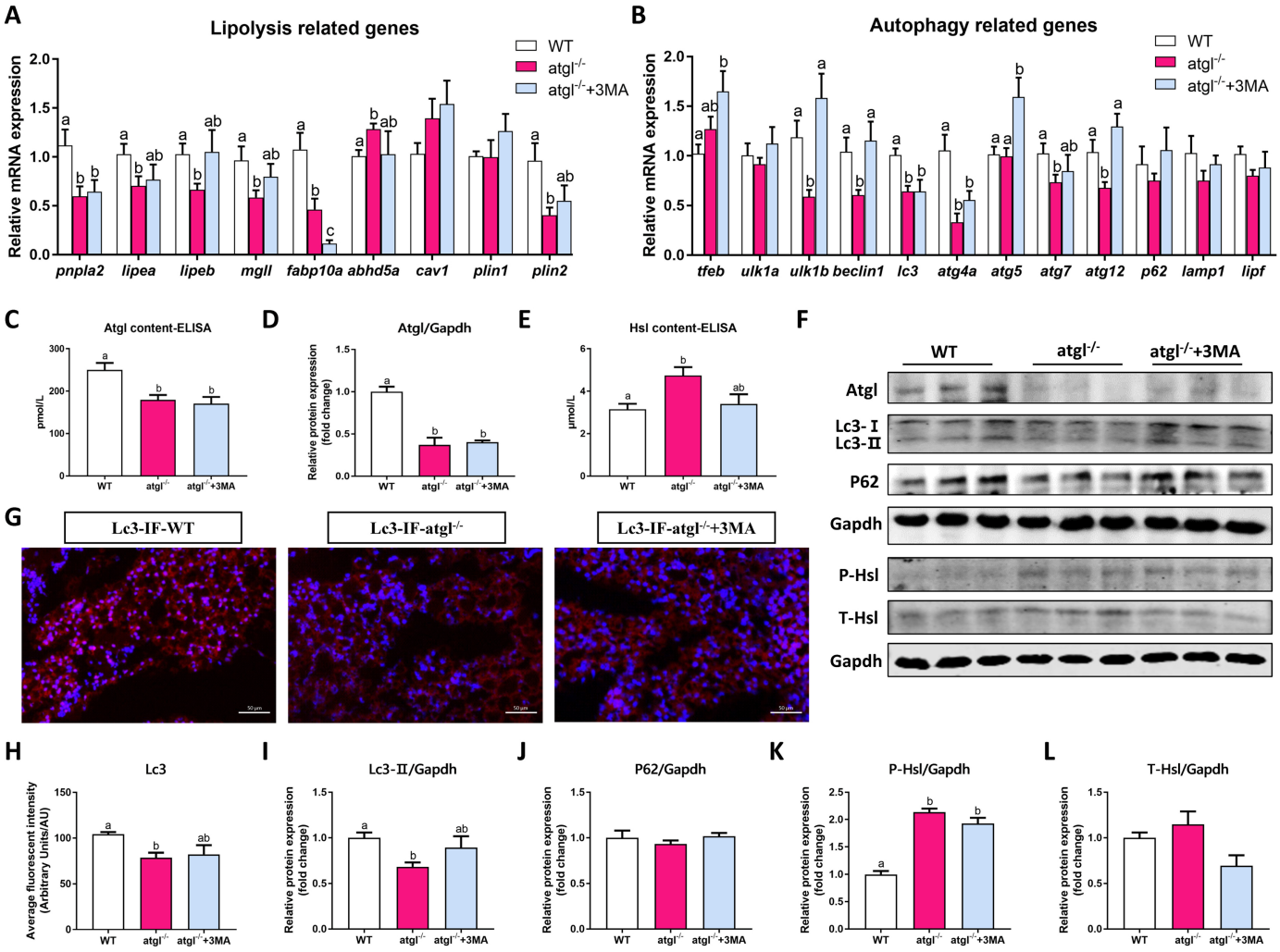

A
Lipolysis related genes
WT
atgl-/-
atgl-/-+3MA
Relative mRNA expression
pnpla2
lipea
lipeb
mgll
fabp10a
abhd5a
cav1
plin1
plin2
B
Autophagy related genes
tfeb
ulk1a
ulk1b
beclin1
lc3
atg4a
atg5
atg7
atg12
p62
lamp1
lipf
C
Atgl content-ELISA
pmol/L
D
Atgl/Gapdh
Relative protein expression (fold change)
E
Hsl content-ELISA
μmol/L
F
Atgl
Lc3-Ⅰ
Lc3-Ⅱ
P62
Gapdh
P-Hsl
T-Hsl
Gapdh
G
Lc3-IF-WT
Lc3-IF-atgl-/-
Lc3-IF-atgl-/-+3MA
H
Lc3
Average fluorescent intensity (Arbitrary Units/AU)
I
Lc3-Ⅱ/Gapdh
J
P62/Gapdh
K
P-Hsl/Gapdh
L
T-Hsl/Gapdh

Figure 5

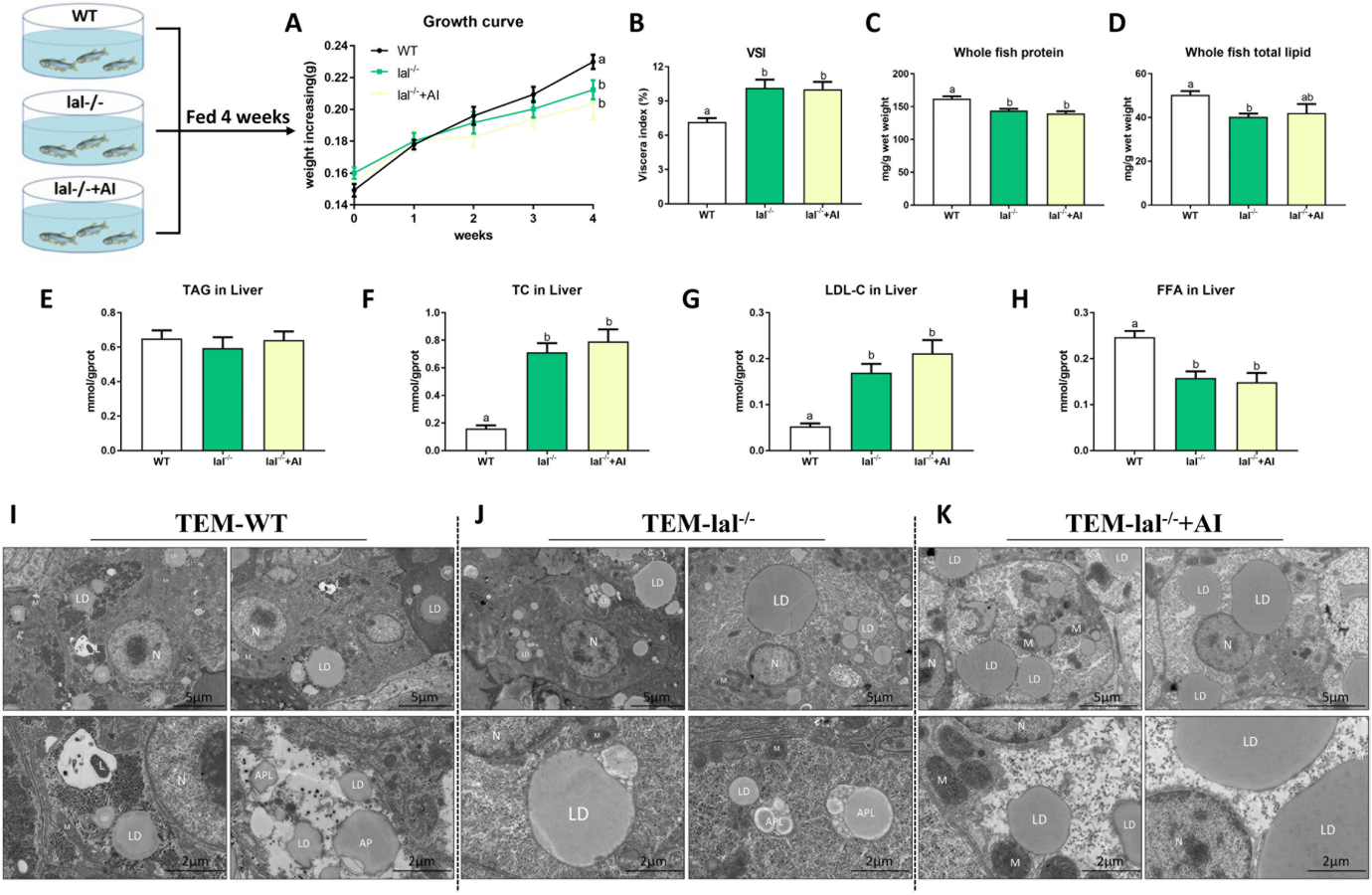

WT
lal-/-
lal-/-+AI
Fed 4 weeks
A
Growth curve
WT
lal-/-
lal-/-+AI
weight increasing(g)
weeks
B
VSI
Viscera index (%)
C
Whole fish protein
mg/g wet weight
D
Whole fish total lipid
mg/g wet weight
E
TAG in Liver
mmol/gprot
F
TC in Liver
mmol/gprot
G
LDL-C in Liver
mmol/gprot
H
FFA in Liver
mmol/gprot
I
TEM-WT
J
TEM-lal-/-
K
TEM-lal-/-+AI
LD
N
M
APL
AP
5μm
2μm

Figure 6

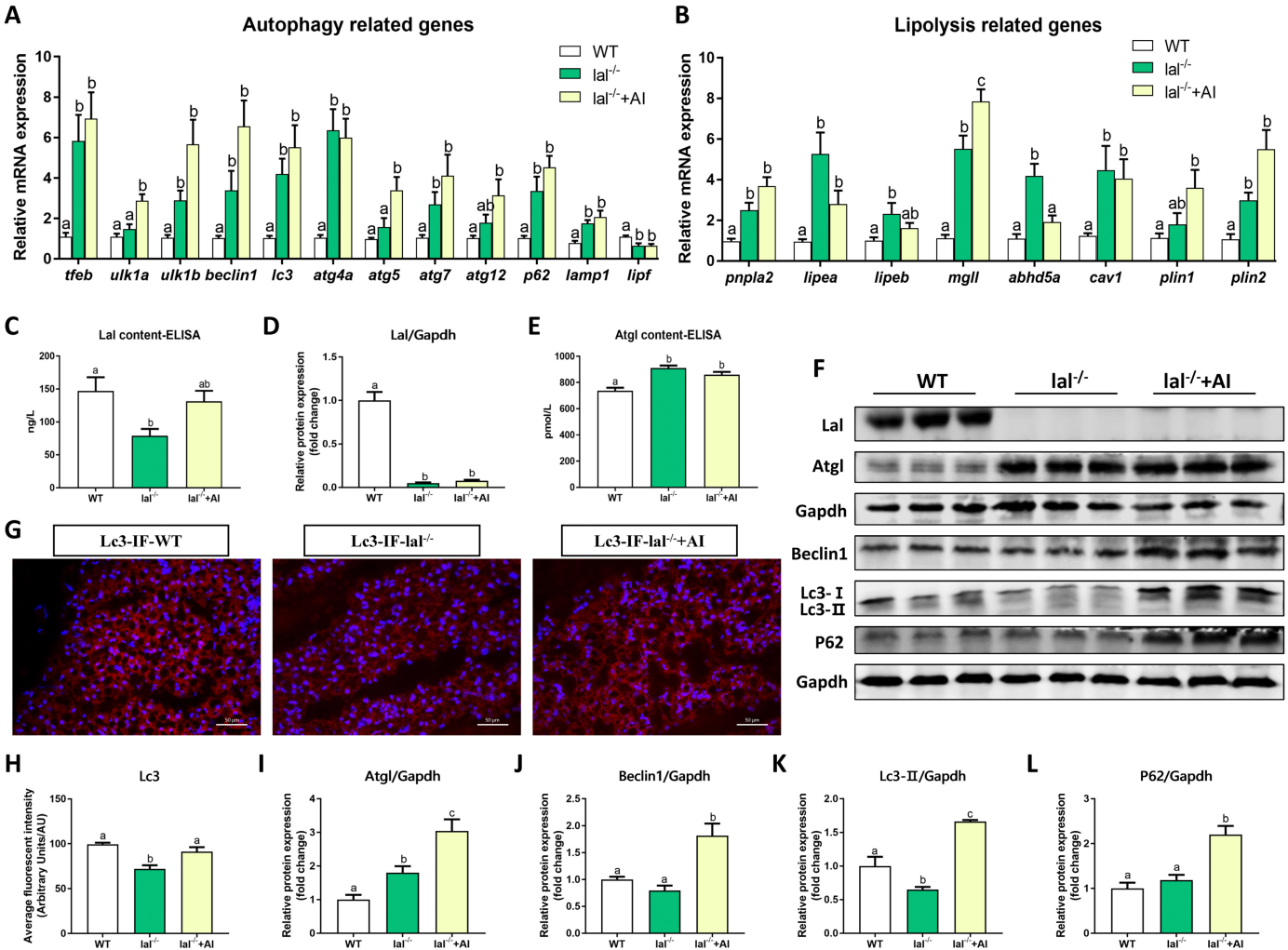

A
Autophagy related genes
Relative mRNA expression
WT
lal-/-
lal-/-+AI
tfeb
ulk1a
ulk1b
beclin1
lc3
atg4a
atg5
atg7
atg12
p62
lamp1
lipf
B
Lipolysis related genes
pnpla2
lipea
lipeb
mgll
abhd5a
cav1
plin1
plin2
C
Lal content-ELISA
ng/L
D
Lal/Gapdh
Relative protein expression (fold change)
E
Atgl content-ELISA
pmol/L
F
Lal
Atgl
Gapdh
Beclin1
Lc3- Ⅰ
Lc3-Ⅱ
P62
G
Lc3-IF-WT
Lc3-IF-lal-/-
Lc3-IF-lal-/-+AI
H
Lc3
Average fluorescent intensity (Arbitrary Units/AU)
I
Atgl/Gapdh
J
Beclin1/Gapdh
K
Lc3-Ⅱ/Gapdh
L
P62/Gapdh

Figure 7

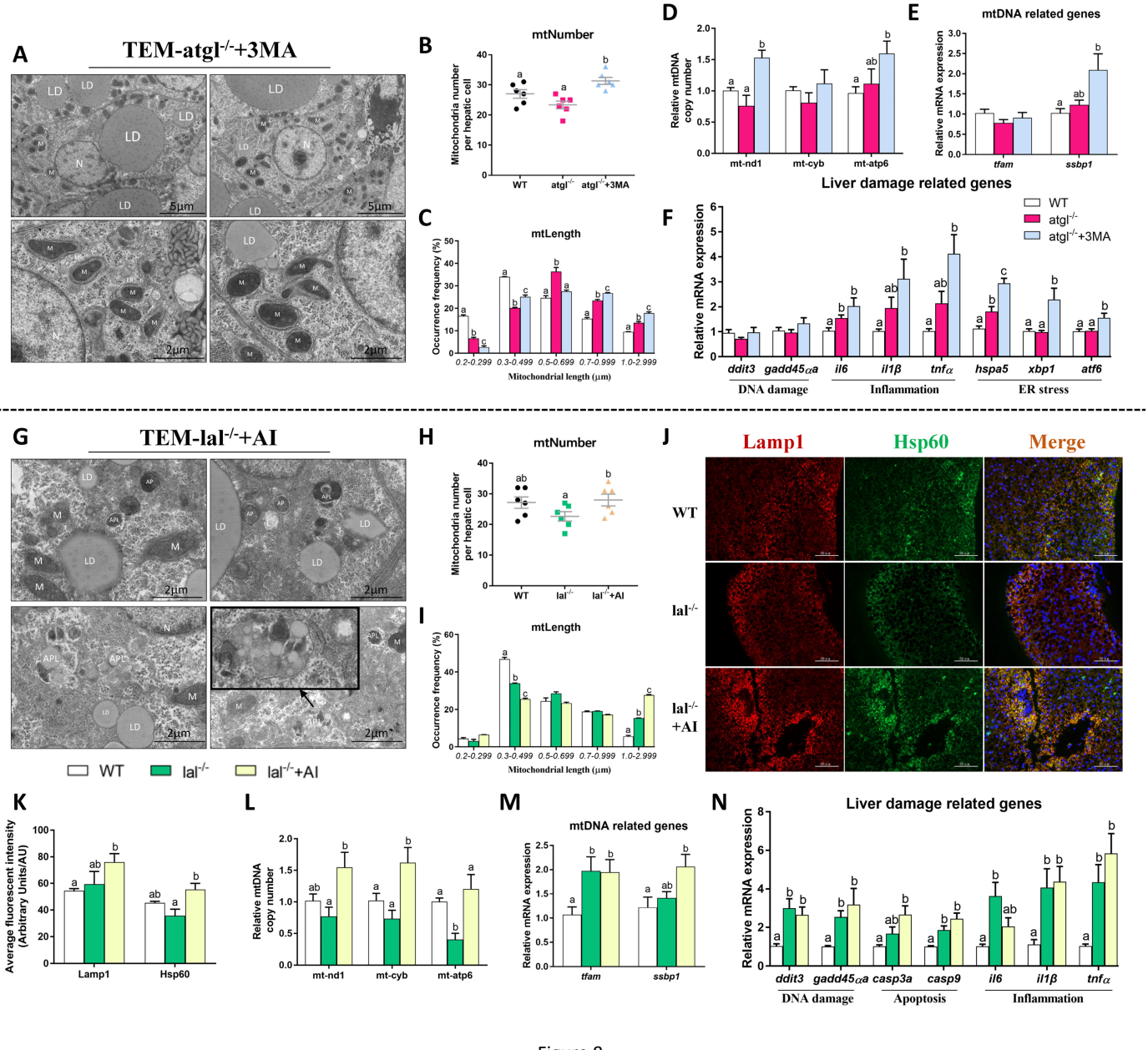

A
TEM-atgl-/-+3MA
LD
N
M
ER
5μm
2μm
B
mtNumber
Mitochondria number per hepatic cell
WT
atgl-/-
atgl-/-+3MA
C
mtLength
Occurrence frequency (%)
0.2-0.299
0.3-0.499
0.5-0.699
0.7-0.999
1.0-2.999
Mitochondrial length (μm)
D
Relative mtDNA copy number
mt-nd1
mt-cyb
mt-atp6
E
mtDNA related genes
Relative mRNA expression
tfam
ssbp1
F
Liver damage related genes
WT
atgl-/-
atgl-/-+3MA
Relative mRNA expression
ddit3
gadd45αa
il6
il1β
tnfα
hspa5
xbp1
atf6
DNA damage
Inflammation
ER stress
G
TEM-lal-/-+AI
AP
APL
LD
M
2μm
WT
lal-/-
lal-/-+AI
H
mtNumber
Mitochondria number per hepatic cell
WT
lal-/-
lal-/-+AI
I
mtLength
Occurrence frequency (%)
0.2-0.299
0.3-0.499
0.5-0.699
0.7-0.999
1.0-2.999
Mitochondrial length (μm)
J
Lamp1
Hsp60
Merge
WT
lal-/-
lal-/-+AI
K
Average fluorescent intensity (Arbitrary Units/AU)
Lamp1
Hsp60
L
Relative mtDNA copy number
mt-nd1
mt-cyb
mt-atp6
M
mtDNA related genes
Relative mRNA expression
tfam
ssbp1
N
Liver damage related genes
Relative mRNA expression
ddit3
gadd45αa
casp3a
casp9
il6
il1β
tnfα
DNA damage
Apoptosis
Inflammation

Figure 8

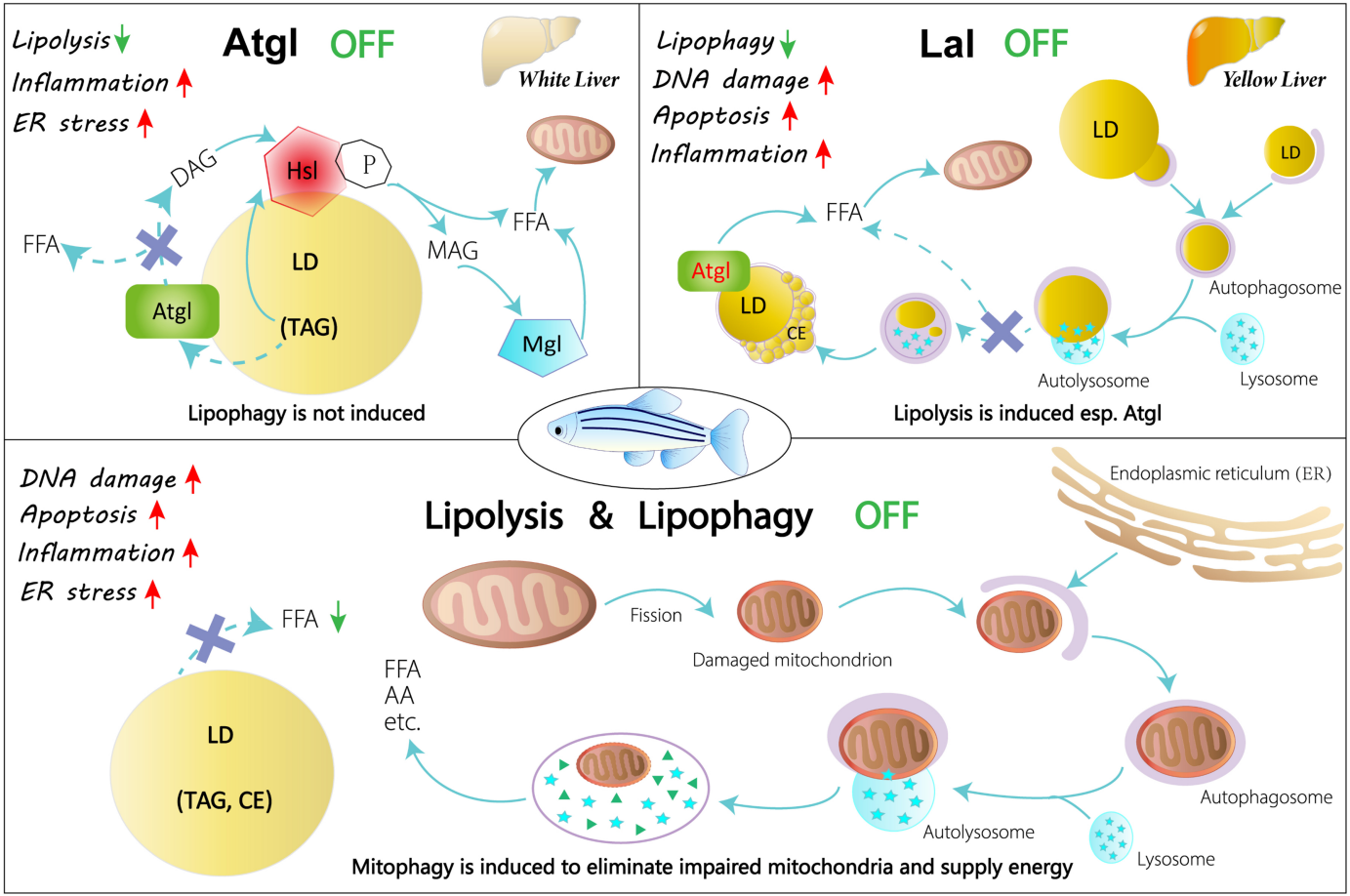

Lipolysis
Inflammation
ER stress
Atgl OFF
White Liver
DAG
Hsl
P
FFA
LD
(TAG)
Atgl
MAG
FFA
Mgl
Lipophagy is not induced
Lipophagy
DNA damage
Apoptosis
Inflammation
Lal OFF
Yellow Liver
LD
LD
FFA
Atgl
LD
CE
Autophagosome
Autolysosome
Lysosome
Lipolysis is induced esp. Atgl
DNA damage
Apoptosis
Inflammation
ER stress
FFA
LD
(TAG, CE)
Lipolysis & Lipophagy OFF
Endoplasmic reticulum (ER)
Fission
Damaged mitochondrion
FFA
AA
etc.
Autophagosome
Autolysosome
Lysosome
Mitophagy is induced to eliminate impaired mitochondria and supply energy

Figure 9